



Baumgartner, M. E., Dinan, M., Langton, P. F., Kucinski, I., & Piddini, E. (2021). Proteotoxic stress is a driver of the loser status and of cell competition. *Nature Cell Biology*, 23(2), 136-146.  
<https://doi.org/10.1038/s41556-020-00627-0>

Peer reviewed version

Link to published version (if available):  
[10.1038/s41556-020-00627-0](https://doi.org/10.1038/s41556-020-00627-0)

[Link to publication record in Explore Bristol Research](#)  
PDF-document

This is the author accepted manuscript (AAM). The final published version (version of record) is available online via Nature Research at <https://doi.org/10.1038/s41556-020-00627-0> . Please refer to any applicable terms of use of the publisher.

## University of Bristol - Explore Bristol Research

### General rights

This document is made available in accordance with publisher policies. Please cite only the published version using the reference above. Full terms of use are available:  
<http://www.bristol.ac.uk/red/research-policy/pure/user-guides/ebr-terms/>

# 1 Proteotoxic stress is a driver of the loser status and of cell competition

2  
3  
4 Michael E. Baumgartner<sup>#1</sup>, Michael P. Dinan<sup>#1,2,§</sup>, Paul F. Langton<sup>1</sup>, Iwo Kucinski<sup>2,§§</sup>, and  
5 Eugenia Piddini<sup>1\*</sup>

## 6 7 8 Affiliations

9 <sup>1</sup> School of Cellular and Molecular Medicine, University of Bristol, Biomedical Sciences  
10 Building, University Walk, Bristol BS8 1TD, UK.

11  
12 <sup>2</sup> The Wellcome Trust/Cancer Research UK Gurdon Institute and Zoology Department,  
13 University of Cambridge, Tennis Court Road, Cambridge CB2 1QN, UK.

14  
15 § Present address: University of Cambridge, UK

16 §§ Present address: Wellcome & MRC Cambridge Stem Cell Institute and Department of  
17 Haematology, University of Cambridge, UK

18  
19  
20 # Joint first authors

21  
22 \* Correspondence should be addressed to EP: [eugenia.piddini@bristol.ac.uk](mailto:eugenia.piddini@bristol.ac.uk)

23  
24 **Keywords:** Cell competition, ribosome mutation, ribosomopathy, proteotoxic stress, autophagy,  
25 proteasome, *Drosophila*, aneuploidy, FOXO, Rapamycin  
26

## Abstract

27  
28  
29  
30  
31  
32  
33  
34  
35  
36  
37  
38  
39  
40  
41  
42

Cell competition allows “winner” cells to eliminate less fit “loser” cells in tissues. In Minute cell competition, cells heterozygous mutant in ribosome genes, such as *RpS3*<sup>+/-</sup> cells, are eliminated by wild-type cells. How cells are primed as losers is partially understood and it has been proposed that reduced translation underpins the loser status of ribosome mutant, or *Minute*, cells. Here, using *Drosophila*, we show that reduced translation does not cause cell competition. Instead, we identify proteotoxic stress as the underlying cause of the loser status for Minute competition and competition induced by *mahjong*, an unrelated loser gene. *RpS3*<sup>+/-</sup> cells exhibit reduced autophagic and proteasomal flux, accumulate protein aggregates, and can be rescued from competition by improving their proteostasis. Conversely, inducing proteotoxic stress is sufficient to turn otherwise wild-type cells into losers. Thus, we propose that tissues may preserve their health through a proteostasis-based mechanism of cell competition and cell selection.

## Introduction

Cell competition is a conserved mechanism that allows “winner” cells to eliminate viable but less fit “loser” cells in tissues<sup>1-3</sup>. This process acts as a mechanism of tissue quality control. By removing mis-specified or damaged cells, cell competition preserves tissue and organism health, potentially delaying ageing and disease onset<sup>4-6</sup>. Furthermore, an increasing body of evidence indicates that competitive interactions contribute to tissue colonisation during cancer growth<sup>7</sup>.

The first form of competition discovered was Minute cell competition, wherein cells heterozygous mutant in ribosome genes are eliminated by neighbouring wild-type cells<sup>1</sup>. Over 80 genes make up the ribosome, and most display a dominant phenotype when mutated or lost, both in *Drosophila* and humans<sup>8,9</sup>. Based both on phenotypic dominance and on the high number of *Minute* genes, spontaneously occurring Minute cell competition is likely to be a frequent event, relative to other types of cell competition. In addition, as ribosome genes are scattered across chromosomes, Minute cell competition may be frequent in diseases characterized by aneuploidy<sup>10</sup>, such as cancer, where deletions of large genomic regions often lead to single copy loss of one or more ribosome genes<sup>11</sup>.

Despite its discovery over 40 years ago<sup>1</sup>, our understanding of the mechanisms of Minute cell competition remains incomplete<sup>12</sup>. While several signals have been identified that act during cell competition<sup>4,13-19</sup>, the upstream signals priming cells as losers are mostly unknown<sup>20</sup>. It is, for instance, unclear how ribosome gene loss leads to the loser status<sup>12</sup>. *Minute* mutants exhibit reduced translation rate<sup>17</sup>, and it has long been assumed that this drives the loser status<sup>18,21-25</sup>. However, the actual contribution of translation has not been investigated.

Here, we investigated how ribosome mutations lead to the loser status. We find that translation is not directly linked to the loser status in Minute competition. Instead, we find that ribosome gene mutations lead to defective autophagy and proteasome flux,

74 accumulation of protein aggregates, and proteotoxic stress. These phenotypes are  
75 causative of the loser status. In addition, inducing proteotoxic stress through  
76 overexpression of aggregate-prone proteins phenocopies these protein catabolism  
77 defects and induces the loser status. Our work identifies proteotoxic stress as the  
78 leading cause of the Minute loser status and implicates cell competition in pathologies  
79 characterized by proteotoxic stress.

80

81

## Results

### Reduced protein synthesis does not confer the loser status

Minute cell competition is characterized by apoptotic elimination of *Minute* loser cells when they are in proximity of wild-type winner cells<sup>1-3</sup>. Thus, although *Minute* *RpS3*<sup>+/-</sup> cells display a modest increase in apoptosis compared to wild-type cells when they are in isolation (Figure 1a-b and<sup>26</sup>), apoptosis is substantially elevated during competition in *RpS3*<sup>+/-</sup> cells that border wild-type cells<sup>12,27,28</sup> (Figure 1c-d). This region-specific induction of apoptosis at clone borders is a hallmark of certain types of cell competition, including Minute competition.

To investigate whether reduced translation triggers cell competition, we expressed a constitutively active form of the translational repressor, 4E-BP (4EBP<sup>TA</sup>)<sup>29,30</sup>, in otherwise wildtype cells. In OPP (O-propargyl-puromycin) and AHA (L-azidohomoalanine) global translation assays, 4EBP<sup>TA</sup> expression induced a reduction in protein synthesis that was comparable to (Figure 1e-g; OPP) or stronger than (Extended Data Figure 1a-c; AHA) that seen in *RpS3*<sup>+/-</sup> cells. 4EBP<sup>TA</sup> expression resulted in little autonomous apoptosis (Figure 1h). Furthermore, the frequency of dying cells was similar at 4EBP<sup>TA</sup> clone borders and clone centers (Figure 1h-i). These data suggest that reducing rates of global protein synthesis alone, at levels equal to or greater than in *RpS3*<sup>+/-</sup> cells, is not sufficient to trigger cell competition and indicate that additional properties induced by *RpS3*<sup>+/-</sup> mutations must also play a role.

We have previously shown that *RpS3*<sup>+/-</sup> cells and cells mutant in the loser gene and ubiquitin ligase *mahjong*<sup>31</sup> (*mahj*), share what we have termed the 'prospective loser status' – a cellular state which predisposes cells to act as losers when confronted with wildtype winners<sup>20</sup>. This state is characterized by activation of a range of stress response pathways, even in the absence of cell competition<sup>20</sup>. For example, *RpS3*<sup>+/-</sup> and *mahj*<sup>-/-</sup> cells display chronic activation of JNK signaling<sup>20,32</sup> and of the Nrf2-mediated oxidative stress response<sup>20</sup>. Furthermore, Nrf2 activation is sufficient to

113 induce the loser status in competition with wild-type cells <sup>20</sup>. To determine whether a  
114 reduction in protein synthesis is sufficient to activate these pathways, we examined the  
115 levels of phospho-JNK and the activation of an Nrf2 reporter, GstD1-GFP, in the  
116 absence of competition <sup>33</sup>. As Minute cell competition does not occur across  
117 compartment boundaries, we are able to use compartment-specific transcriptional  
118 drivers to generate wing discs with two distinct but non-competing cell populations, one  
119 in the anterior compartment and one in the posterior. Similarly to *RpS3<sup>+/-</sup>* cells, the  
120 levels of phospho-JNK were higher in wing disc cells expressing 4EBP<sup>TA</sup> than in the  
121 wild-type compartment (Figure 1j-k). However, GstD1-GFP levels were only minimally  
122 affected in 4EBP<sup>TA</sup> cells (Figure 1l-n). Thus, a reduction in protein synthesis can  
123 produce some aspects of the prospective loser status (JNK activation) but is insufficient  
124 to induce oxidative stress response activity or provoke cell competition.

125 We next asked whether reduced protein synthesis is necessary for *mahj<sup>-/-</sup>* cells or  
126 *RpS3<sup>+/-</sup>* cells to behave as losers. Knock-down of Mahj did not affect protein translation  
127 rate (Extended Data Figure 1d-e), indicating that translation inhibition does not play a  
128 role in priming *mahj<sup>-/-</sup>* cells as losers. Next, we sought to boost rates of translation in  
129 *RpS3<sup>+/-</sup>* cells and assess the resulting effect on the prospective loser status and on  
130 Minute competition. GADD34 can stimulate translation via dephosphorylation of the  
131 translation initiation factor, eIF2 $\alpha$  <sup>34</sup>. Indeed, GADD34 overexpression in *RpS3<sup>+/-</sup>* cells  
132 caused a reduction in phospho-eIF2 $\alpha$  (Extended Data Figure 1f-g) and a corresponding  
133 rescue of translation, as assessed by OPP incorporation (Figure 1o-p). Surprisingly,  
134 GADD34-expressing *RpS3<sup>+/-</sup>* cells displayed higher levels of the GstD1-GFP oxidative  
135 stress reporter (Extended Data Figure 1h-i) and performed worse than *RpS3<sup>+/-</sup>* cells in  
136 competition, with hardly any surviving at the point of dissection (Figure 1q-s). Thus,  
137 translation inhibition seems to counter the loser status rather than contribute to it, in  
138 *RpS3<sup>+/-</sup>* cells.

139

#### 140 **Prospective losers display dependence on autophagy and defective autophagic** 141 **flux**

142

143 In order to seek out an alternative cause of the prospective loser status, we  
144 turned to a known rescue of Minute competition: inhibition of JNK signaling. In addition  
145 to rescuing *RpS3*<sup>+/-</sup> cells from competition, JNK inhibition partially reverses activation of  
146 the transcriptional signature associated with prospective losers<sup>20</sup>. Furthermore, it  
147 reduces GstD1-GFP reporter activation in *RpS3*<sup>+/-</sup> cells (Extended Data Figure 2a).  
148 Thus, we compared the transcriptional profiles of *RpS3*<sup>+/-</sup> wing discs with or without JNK  
149 signaling inhibition<sup>20</sup>, to identify pathways associated with JNK inhibition and with a  
150 rescue of the loser status. This revealed differential expression of genes involved in  
151 protein catabolism, the proteasome, autophagy, and the unfolded protein response  
152 (Supplementary Table 1). These pathways have all been implicated in Nrf2 regulation  
153<sup>35,36</sup>, supporting a potential role in cell competition.

154  
155 In order to examine the role of autophagy in *RpS3*<sup>+/-</sup> cells, we obtained wing  
156 discs from larvae carrying heterozygous mutations for both *RpS3* and one of several  
157 autophagy-related genes: *p62* (*ref(2)P* in *Drosophila*), *atg8* or *atg13*<sup>37</sup>. We found that all  
158 three autophagy mutations caused a cell-autonomous increase in apoptotic events in an  
159 *RpS3*<sup>+/-</sup> background, as compared to *RpS3*<sup>+/-</sup> or autophagy mutations alone (Figure 2a-  
160 b, Extended Data Figure 2b-d). Heterozygous mutations in another ribosome loser  
161 mutation, *RpL27A*, also caused increased apoptosis in combination with heterozygous  
162 mutations in the autophagy gene *p62* (Extended Data Figure 2e-f). Thus, *Minute* cells  
163 are acutely reliant on autophagy. However, autophagy inhibition did not impact the  
164 competitive status of *RpS3*<sup>+/-</sup> cells, as knockdown of autophagy genes *atg1* or *atg9* by  
165 RNAi did not affect clone coverage or competition-induced cell death in competing  
166 *RpS3*<sup>+/-</sup> cells (except for a mild increase in competitive death in the case of *atg1* RNAi;  
167 Extended Data Figure 2g-i). This contrasts with data from Nagata et al.,<sup>18</sup> who have  
168 instead shown that inhibiting autophagy rescues *Minute* cells from competition. Non-  
169 competing *RpS3*<sup>+/-</sup> cells also appeared to have more *atg8*-positive foci (Figure 2c) and  
170 had more *p62*-positive foci (Figure 2d-e) than wild-type cells.

171  
172 Cells with reduced function of the loser gene and ubiquitin ligase *mahj* share with  
173 *RpS3*<sup>+/-</sup> cells a cell-autonomous signature of hundreds of differentially expressed genes



174 relative to wild-type cells, as well as a cell-autonomous activation of the oxidative stress  
175 response<sup>20</sup>. This suggests that mutations in *mahj* and *RpS3* lead to cell competition  
176 using a convergent mechanism<sup>20</sup>. Thus, we examined the autophagic state in *mahj*<sup>-/-</sup>  
177 cells. *mahj*<sup>-/-</sup> homozygous clones in a background of *mahj*<sup>+/-</sup> and wild type cells also  
178 accumulated p62 foci (Figure 2f), whereas 4EBP<sup>TA</sup> had no effect on the number of p62  
179 foci (Figure 2g). Thus, deregulated autophagy is associated with the prospective loser  
180 status of two functionally unrelated mutants, and this is not a consequence of reduced  
181 protein synthesis.

182

183 Accumulation of Atg8- and p62-positive autophagosomes can reflect either  
184 decreased or increased autophagic flux<sup>38</sup>. To measure autophagic flux in prospective  
185 losers, we designed the reporter “ReFlux” (Ref(2)P autophagy Flux) that measures the  
186 rate of p62 degradation<sup>38,39</sup>. p62 is both an autophagy adaptor and an autophagy cargo  
187 that is degraded upon autophagosome degradation by the lysosome<sup>38</sup>. Thus,  
188 measuring the rate of p62 degradation provides a direct measure of autophagic flux<sup>38</sup>.  
189 In ReFlux, p62 is fused to GFP and driven by a *heat-shock (hs)* promoter for pulse-  
190 chase expression<sup>40</sup> (Figure 2h). As a control, we confirmed that ReFlux reports reduced  
191 autophagic flux upon depletion of the autophagy gene *atg1* (Extended Data Figure 3a-  
192 c). Then, we expressed ReFlux across wing discs containing *RpS3*<sup>+/-</sup> anterior and wild-  
193 type posterior compartments. We found that *RpS3*<sup>+/-</sup> and wild-type cells show similar  
194 GFP-p62 ReFlux signal intensity immediately following pulse expression. However, after  
195 a chase period, GFP-p62 ReFlux signal perdures in *RpS3*<sup>+/-</sup> cells compared to wild-type  
196 cells, indicating reduced autophagic flux (Figure 2i-k). A reduced autophagic flux was  
197 also seen in competing *RpS3*<sup>+/-</sup> cells, relative to competing wild-type cells (Extended  
198 Data Figure 3d-f). Treatment with the autophagy inhibitor chloroquine led to persistence  
199 of the GFP-p62 ReFlux signal, confirming that GFP-p62 ReFlux loss is due to  
200 autophagic degradation (Extended Data Figure 3g). ReFlux was eventually cleared from  
201 the *RpS3*<sup>+/-</sup> compartment (Extended Data Figure 3h), indicating that autophagic  
202 degradation is delayed but not blocked. Knockdown of Mahj also reduced autophagic  
203 flux (Figure 2l-n). Overexpression of 4EBP<sup>TA</sup> also reduced autophagic flux, albeit with a  
204 substantially smaller effect size than *RpS3*<sup>+/-</sup> mutations (Extended Data Figure 3i-k).

205

206

### **Defective autophagy does not cause the loser status**

207

208 Defective autophagy has been associated with the loser status in mouse  
209 embryonic stem cells <sup>41</sup>. Having observed reduced autophagic flux in both *RpS3*<sup>+/-</sup> and  
210 *mahj*<sup>-/-</sup> prospective losers, we next investigated whether reduced autophagy is sufficient  
211 to induce the loser status in these epithelia. Clones of cells expressing *atg1* RNAi within  
212 wild-type imaginal discs did not show cell death enrichment at the clone borders (Figure  
213 3a-b), even though they accumulated p62 foci (Figure 3c), indicative of impaired  
214 autophagy. *atg1*-depleted cells also failed to activate the oxidative stress response in a  
215 non-competitive context (Figure 3d, right), despite confirmation of autophagy  
216 impairment from p62 accumulation (Figure 3d, left). Similarly, inhibiting autophagy in  
217 clones by mutating *atg13* caused accumulation of p62 foci (Figure 3e), but did not result  
218 in cell competition with wild-type cells, as neither cell death nor clonal disadvantage  
219 were observed (Figure 3f-h). Therefore, reduced autophagic flux is observed in *RpS3*<sup>+/-</sup>  
220 cells both in the absence of and during competition but is not sufficient to cause cell  
221 competition.

222

223 As reduced protein synthesis and autophagy flux are observed in *RpS3*<sup>+/-</sup> losers  
224 but neither is sufficient to confer the loser status, we asked whether they might do so in  
225 concert. However, co-expressing *atg9* RNAi and 4EBP<sup>TA</sup> in clones of cells in a wild-type  
226 wing disc did not result in border cell death, indicating that reduced protein synthesis  
227 and defective autophagy together are not sufficient to induce the competitive elimination  
228 of losers (Figure 3i-k).

229

230

### **Prospective losers have defective proteasome flux**

231

232 Proteasome genes were also differentially expressed in *RpS3*<sup>+/-</sup> cells upon JNK  
233 signaling inhibition (Supplementary Table 1), prompting us to investigate the role of the  
234 proteasome in *Minute* cells. Heterozygosity of a proteasomal core subunit gene caused  
235 increased apoptosis in *RpS3*<sup>+/-</sup> cells and in *RpL27A*<sup>+/-</sup> cells (Extended Data Figure 4a-

236 d). Similarly, feeding flies the proteasome inhibitor bortezomib<sup>42</sup> increased the number  
237 of dying cells in *RpS3*<sup>+/-</sup> but not wild-type wing discs (Figure 4a-c). Thus, ribosome  
238 mutant cells are cell-autonomously reliant on proteasome function in addition to  
239 autophagy.

240

241 To determine whether proteasome function is dysregulated in *RpS3*<sup>+/-</sup> cells, we  
242 examined proteasome activity with CL1-GFP, a fusion of GFP with the proteasome  
243 degradation signal CL1, which targets GFP for efficient proteasomal degradation<sup>43</sup>. To  
244 enhance reporter sensitivity, we designed the reporter ProteoFlux, a *hs*-driven CL1-  
245 GFP, to enable pulse-chase measurements of proteasome flux (Figure 4d). We  
246 confirmed that ProteoFlux CL1-GFP detects reduced proteasome flux when we interfere  
247 with proteasome function by knockdown of the proteasome subunit Rpt6 (Figure 4e-f).  
248 We then expressed ProteoFLUX CL1-GFP in wing discs harboring *RpS3*<sup>+/-</sup> anterior and  
249 wild-type posterior compartments, so that we could compare directly their proteasome  
250 flux in the absence of cell competition. *RpS3*<sup>+/-</sup> and wild-type cells showed similar  
251 ProteoFLUX CL1-GFP signal intensity immediately after pulse expression. After a chase  
252 period, however, we observed higher GFP intensity in *RpS3*<sup>+/-</sup> than in wild-type cells,  
253 indicating slower proteasome flux in *RpS3*<sup>+/-</sup> cells (Figure 4g-i). ProteoFlux CL1-GFP  
254 degradation was also delayed in cells depleted for Mahj (Extended Data Figure 4e-g),  
255 but not in 4EBP<sup>TA</sup>-expressing cells (Extended Data Figure 4h-j). Therefore, like reduced  
256 autophagic flux, reduced proteasomal flux is a common feature of genetically distinct  
257 prospective losers.

258

259 ***RpS3*<sup>+/-</sup> mutations induce protein aggregates and stoichiometric imbalance**  
260 **in ribosome proteins**

261

262 Ribosomal proteins are degraded by the proteasome<sup>44</sup> and by autophagy<sup>45,46</sup>.  
263 Indeed, electron microscopy analysis showed phago-lysosomal structures containing  
264 ribosomes both in wild-type and in *RpS3*<sup>+/-</sup> wing disc cells (Extended Data Figure 4k).  
265 We reasoned that *RpS3*<sup>+/-</sup> mutations could lead to a stoichiometric imbalance in  
266 ribosome proteins, which could in turn cause proteotoxic stress and overload the

267 proteasome and autophagy machineries<sup>47,48</sup>. To test this, we measured relative levels  
268 of ribosome proteins, by Tandem Mass Tag (TMT) Spectrometry of *RpS3<sup>+/-</sup>* and wild-  
269 type wing discs. TMT successfully identified 78 ribosome proteins of the 93 reported on  
270 Flybase (of the missing 15, 8 are not expected to be expressed in wing discs). This  
271 showed that the *RpS3<sup>+/-</sup>* mutation causes a reduction in RpS3 protein of 0.291 log-fold  
272 relative to wild-type levels. Interestingly, a reduction was observed for all small  
273 ribosome subunit proteins detected (Figure 4j), indicating coordinated regulation, but  
274 this was not seen for components of the large subunit, whose levels were, with few  
275 exceptions, equal to or higher than in wild-type cells (Figure 4j). Thus, at steady state,  
276 *RpS3<sup>+/-</sup>* cells have a stoichiometric excess of ribosome proteins from the large subunit  
277 relative to small subunit ribosome proteins. This could contribute to proteasome and  
278 autophagy overload.

279

280 When they are not efficiently cleared by degradation, ribosome proteins can form  
281 protein aggregates<sup>44,47,48</sup>. To test this, we used Proteostat, a dye which fluoresces upon  
282 intercalation with protein aggregate-associated quaternary structures. Indeed,  
283 Proteostat staining detected accumulation of protein aggregates in *RpS3<sup>+/-</sup>* cells relative  
284 to wild-type cells, in the absence of cell competition (Figure 4k). Protein aggregates are  
285 often ubiquitin-positive<sup>49,50</sup>, and immunostaining with the FK2 antibody, which detects  
286 mono- and poly-ubiquitin conjugates, revealed that *RpS3<sup>+/-</sup>* cells, but not wild-type cells,  
287 accumulate large, ubiquitin-positive foci in the cytoplasm (Figure 4l). Many of these foci  
288 were also positive for the autophagy adapter/cargo p62 (Figure 4l), which is often  
289 recruited to cytosolic protein aggregates<sup>50</sup>. Furthermore, phospho-eIF2 $\alpha$ , a marker of  
290 proteotoxic stress and of the integrated stress response<sup>34</sup>, was upregulated in *RpS3<sup>+/-</sup>*  
291 cells, both in homotypic conditions (Extended Data Figure 4l-m) and during cell  
292 competition (Extended Data Figure 4n-o). Collectively, *RpS3<sup>+/-</sup>* cells show reduced  
293 autophagy flux, reduced proteasome flux, accumulation of ubiquitinated protein  
294 aggregates, and markers of proteotoxic stress.

295

296

297 **Improving proteostasis in *RpS3<sup>+/-</sup>* cells rescues their loser status**

298

299

300 Proteotoxic stress can induce Nrf2 activation <sup>51</sup>, and this in turn is linked to the  
301 loser status <sup>20</sup>, suggesting a link between proteotoxic stress and the prospective loser  
302 status. Consistent with this, inhibiting the proteasome with bortezomib was sufficient to  
303 elevate GstD1-GFP signal in non-competing wild-type and *RpS3*<sup>+/-</sup> wing disc cells  
304 (Extended Data Figure 5a-c). We therefore asked whether alleviating proteotoxic stress  
305 would rescue loser cells from competition. Rapamycin inhibits TOR signaling and  
306 promotes proteostasis via multiple mechanisms, including inhibiting translation and  
307 activating autophagy and proteasome functions <sup>52,53</sup>. We found that rapamycin feeding  
308 reduced the frequency of competition-induced apoptosis in *RpS3*<sup>+/-</sup> cells bordering wild-  
309 type cells (Figure 5a-c). Rapamycin feeding also reduced the cell-autonomous  
310 activation of the oxidative stress reporter GstD1-GFP in *RpS3*<sup>+/-</sup> cells (Figure 5d-e). As  
311 rapamycin was fed systemically, the observed rescue of competition-induced cell death  
312 could in part arise from the effects of rapamycin on wild-type cells. We therefore sought  
313 to improve proteostasis specifically in *RpS3*<sup>+/-</sup> cells. To this end, we overexpressed, in  
314 *RpS3*<sup>+/-</sup> cells, the transcription factor FOXO, which is inhibited by TOR signaling <sup>54,55</sup>  
315 and promotes both autophagy and proteasome functions <sup>55</sup>. FOXO overexpression  
316 reduced the number of p62-positive aggregates (Figure 5f), increased protein synthesis  
317 (Figure 5g-h) and reduced mildly the levels of phospho-eIF2 $\alpha$  (Figure 5i-j) in *RpS3*<sup>+/-</sup>  
318 cells, indicating overall improved proteostasis. Strikingly, FOXO overexpression in  
319 *RpS3*<sup>+/-</sup> cells abolished competition-induced cell death, as very few apoptotic bodies  
320 could be detected in competition with wild-type cells (Figure 5k-m). These data indicate  
321 that reducing proteotoxic stress inhibits the competitive elimination of *RpS3*<sup>+/-</sup> cells.

322

323

### **Proteotoxic stress is sufficient to cause the loser status**

324

325 We considered that protein aggregation and proteotoxic stress could be sufficient  
326 to cause the loser status in competitive contexts. To test this hypothesis, we ectopically  
327 expressed the human aggregate-prone polyQ protein ataxin-3 (SCA3/MJDQ78), which  
328 is responsible for the human neurodegenerative disorder Machado Joseph Disease <sup>56</sup>

329 and has been used in *Drosophila* to model this neurodegenerative condition<sup>57</sup>. MJDQ78  
330 expression was sufficient to recapitulate many features shared by *RpS3*<sup>+/-</sup> and *mahj*<sup>+/-</sup>  
331 prospective losers, namely up-regulation of GstD1-GFP (Figure 6a-b), reduced  
332 autophagic flux (Figure 6c), and accumulation of p62-positive structures (Figure 6d-e).  
333 MJDQ78 however, did not perceptibly impact on rates of translation, as measured by  
334 OPP incorporation (Figure 6f-g). Importantly, clones overexpressing MJDQ78 in wild-  
335 type wing disc showed a local induction of apoptosis, specifically at their borders with  
336 wild-type cells (Figure 6h-i), and grew poorly relatively to wild-type clones (Figure 6j-l),  
337 indicating that these cells are eliminated by cell competition. This was specifically  
338 induced by proteotoxic stress, as clones expressing the wild-type version of Ataxin-3  
339 (MJDQ27)<sup>57</sup> did not show induction of border death (Extended Data Figure 5d-f). Thus,  
340 proteotoxic stress is sufficient to turn otherwise wild-type cells into losers (Figure 6m).  
341

## Discussion

342  
343

344 Our work shows that single copy loss of ribosome genes leads to major defects  
345 in cellular proteostasis, as also shown in the accompanying paper from Recances-  
346 Alvarez et al.,<sup>58</sup>. Heterozygosity of ribosome genes in humans leads to genetic  
347 disorders collectively known as ribosomopathies, characterized by severe  
348 malformations and pathologies<sup>9</sup>. The mechanisms through which ribosomal mutations  
349 lead to these defects are only partially understood<sup>9</sup>. Our work suggests that proteotoxic  
350 stress may be an underlying cause for some such defects and that they might be  
351 improved by drugs that promote proteostasis, such as the FDA-approved compound  
352 rapamycin<sup>53</sup> that we have used in this study.

353

354 Our work shows that proteotoxic stress is sufficient to confer the loser status.  
355 This finding broadens the scope of cell competition and suggests it may be an active  
356 mechanism in physiological and pathological contexts characterized by proteotoxic  
357 stress. This may help explain the competitive elimination of neurons in *Drosophila*  
358 models of neurodegenerative diseases<sup>59</sup>. It may be especially relevant to cancer,  
359 where proteotoxic stress is often observed<sup>60</sup>. Our findings suggest that cancer cells  
360 might represent concealed losers that have escaped proteotoxic stress-induced cell  
361 competition through masking mutations. Understanding how *Minute* mutations and  
362 proteotoxic stress lead to cell competition may help unmask the loser status in cancer  
363 cells in ways that could be exploited therapeutically<sup>7</sup>.

364

365 Healthy proteostasis is a driver of organism fitness<sup>61</sup> and contributes to organism  
366 longevity<sup>62</sup>, whereas impaired proteostasis is associated with aging and with age-  
367 related pathologies<sup>62, 63</sup>. We propose that tissues preserve their health and youth  
368 through a proteostasis-based mechanism of cell elimination. By measuring cell fitness  
369 on the basis of proteostasis and converting it into the loser status through the activation  
370 of the oxidative stress response, proteostasis-based cell competition could act as a  
371 general mechanism of cell selection in adult homeostasis. How proteotoxic stress  
372 induces the loser status remains to be established.

## Acknowledgments

373

374

375 We thank the Piddini group for input on the project and manuscript, Rafael Carazo  
376 Salas for feedback and discussions on the data and Life Science Editors for editorial  
377 assistance. We thank the Wolfson Bioimaging Facility for access to microscopes and for  
378 assistance in performing electron microscopy. We also thank the University of Bristol  
379 Proteomics Facility for performing the TMT proteomic experiments and for proteomics  
380 bioinformatics support. We are grateful to Tor Erik Rusten for the generous gift of the  
381 p62 antibody. This work was supported by Wellcome Trust PhD studentships to MPD  
382 and to IK, a Cancer Research UK Programme Grant to E.P. (A12460), a Cancer  
383 Research UK Programme Foundation Award to E.P. (Grant C38607/A26831) and a  
384 Royal Society University Research fellowship to E.P. (UF0905080). E.P. is a Wellcome  
385 Trust Senior Research Fellow (205010/Z/, 16/Z).

386

387 **Author contributions:** E.P. led the project. All authors conceived the experiments.  
388 M.P.D, M.B, I.K. and P.F.L performed and analysed the experiments. M.P.D, M.B, P.F.L  
389 and E.P. wrote the manuscript.

390

391 **Financial and non-financial competing interests:** The authors declare no competing  
392 interests.

393

394 **Materials & correspondence:** The Lead Contact, Eugenia Piddini  
395 (ep16996@bristol.ac.uk), will fulfil requests for resources and reagents.

396



## References

- 397  
398  
399 1. Morata, G. & Ripoll, P. Minutes: mutants of drosophila autonomously affecting cell  
400 division rate. *Developmental Biology* **42**, 211–221 (1975).  
401 2. Baker, N. E. Mechanisms of cell competition emerging from Drosophila studies.  
402 *Curr. Opin. Cell Biol.* **48**, 40–46 (2017).  
403 3. Maruyama, T. & Fujita, Y. Cell competition in mammals - novel homeostatic  
404 machinery for embryonic development and cancer prevention. *Curr. Opin. Cell*  
405 *Biol.* **48**, 106–112 (2017).  
406 4. Merino, M. M. *et al.* Elimination of unfit cells maintains tissue health and prolongs  
407 lifespan. *Cell* **160**, 461–476 (2015).  
408 5. Brown, S. *et al.* Correction of aberrant growth preserves tissue homeostasis.  
409 *Nature* **548**, 334–337 (2017).  
410 6. Liu, N. *et al.* Stem cell competition orchestrates skin homeostasis and ageing.  
411 *Nature* **568**, 344–350 (2019).  
412 7. Vishwakarma, M. & Piddini, E. Outcompeting cancer. *Nature Reviews Cancer* **20**,  
413 187–198 (2020).  
414 8. Marygold, S. J. *et al.* The ribosomal protein genes and Minute loci of Drosophila  
415 melanogaster. *Genome Biol* **8**, R216 (2007).  
416 9. Mills, E. W. & Green, R. Ribosomopathies: There's strength in numbers. *Science*  
417 **358**, eaan2755 (2017).  
418 10. Baker, N. E. Cell competition. *Curr. Biol.* **21**, R11–5 (2011).  
419 11. Ajore, R. *et al.* Deletion of ribosomal protein genes is a common vulnerability in  
420 human cancer, especially in concert with TP53 mutations. *EMBO Mol Med* **9**,  
421 498–507 (2017).  
422 12. Baker, N. E. Emerging mechanisms of cell competition. *Nat. Rev. Genet.* **29**, 1–15  
423 (2020).  
424 13. Rhiner, C. *et al.* Flower Forms an Extracellular Code that Reveals the Fitness of a  
425 Cell to its Neighbors in Drosophila. *Dev. Cell* **18**, 985–998 (2010).  
426 14. Meyer, S. N. *et al.* An ancient defense system eliminates unfit cells from  
427 developing tissues during cell competition. *Science* **346**, 1258236 (2014).  
428 15. Baillon, L., Germani, F., Rockel, C., Hilchenbach, J. & Basler, K. Xrp1 is a  
429 transcription factor required for cell competition-driven elimination of loser cells.  
430 *Sci Rep* **8**, 17712–10 (2018).  
431 16. Kale, A., Li, W., Lee, C.-H. & Baker, N. E. Apoptotic mechanisms during  
432 competition of ribosomal protein mutant cells: roles of the initiator caspases Dronc  
433 and Dream/Strica. *Cell Death Differ* **22**, 1300–1312 (2015).  
434 17. Lee, C.-H. *et al.* A Regulatory Response to Ribosomal Protein Mutations Controls  
435 Translation, Growth, and Cell Competition. *Dev. Cell* **46**, 456–469.e4 (2018).  
436 18. Nagata, R., Nakamura, M., Sanaki, Y. & Igaki, T. Cell Competition Is Driven by  
437 Autophagy. *Dev. Cell* **51**, 99–112.e4 (2019).  
438 19. Blanco, J., Cooper, J. C. & Baker, N. E. Roles of C/EBP class bZip proteins in the  
439 growth and cell competition of Rp ('Minute') mutants in Drosophila. *Elife* **9**, 5184  
440 (2020).

- 441 20. Kucinski, I., Dinan, M., Kolahgar, G. & Piddini, E. Chronic activation of JNK  
442 JAK/STAT and oxidative stress signalling causes the loser cell status. *Nature*  
443 *Communications* **8**, 136 (2017).
- 444 21. Kale, A. *et al.* Ribosomal Protein S12e Has a Distinct Function in Cell  
445 Competition. *Dev. Cell* **44**, 42–55.e4 (2018).
- 446 22. Lee, C.-H. *et al.* A Regulatory Response to Ribosomal Protein Mutations Controls  
447 Translation, Growth, and Cell Competition. *Dev. Cell* **46**, 807 (2018).
- 448 23. Milán, M. Survival of the fittest. Cell competition in the Drosophila wing. *EMBO*  
449 *reports* **3**, 724–725 (2002).
- 450 24. Moreno, E. & Basler, K. dMyc transforms cells into super-competitors. *Cell* **117**,  
451 117–129 (2004).
- 452 25. Amoyel, M. & Bach, E. A. Cell competition: how to eliminate your neighbours.  
453 *Development* **141**, 988–1000 (2014).
- 454 26. Coelho, C. M. A. Growth and cell survival are unevenly impaired in pixie mutant  
455 wing discs. *Development* **132**, 5411–5424 (2005).
- 456 27. Moreno, E., Basler, K. & Morata, G. Cells compete for decapentaplegic survival  
457 factor to prevent apoptosis in Drosophila wing development. *Nature* **416**, 755–759  
458 (2002).
- 459 28. Li, W. & Baker, N. E. Engulfment is required for cell competition. *Cell* **129**, 1215–  
460 1225 (2007).
- 461 29. Imai, Y. *et al.* Phosphorylation of 4E-BP by LRRK2 affects the maintenance of  
462 dopaminergic neurons in Drosophila. *The EMBO Journal* **27**, 2432–2443 (2008).
- 463 30. Mader, S., Lee, H., Pause, A. & Sonenberg, N. The translation initiation factor  
464 eIF-4E binds to a common motif shared by the translation factor eIF-4 gamma  
465 and the translational repressors 4E-binding proteins. *Molecular and Cellular*  
466 *Biology* **15**, 4990–4997 (1995).
- 467 31. Tamori, Y. *et al.* Involvement of Lgl and Mahjong/VprBP in Cell Competition. *Plos*  
468 *Biol* **8**, e1000422 (2010).
- 469 32. Tamori, Y. & Deng, W.-M. Cell competition and its implications for development  
470 and cancer. *Journal of Genetics and Genomics* **38**, 483–495 (2011).
- 471 33. Sykiotis, G. P. & Bohmann, D. Keap1/Nrf2 signaling regulates oxidative stress  
472 tolerance and lifespan in Drosophila. *Dev. Cell* **14**, 76–85 (2008).
- 473 34. Pakos-Zebrucka, K. *et al.* The integrated stress response. *EMBO reports* **17**,  
474 1374–1395 (2016).
- 475 35. Jain, A. *et al.* p62/Sequestosome-1, Autophagy-related Gene 8, and Autophagy in  
476 Drosophila Are Regulated by Nuclear Factor Erythroid 2-related Factor 2 (NRF2),  
477 Independent of Transcription Factor TFEB. *Journal of Biological Chemistry* **290**,  
478 14945–14962 (2015).
- 479 36. Silva-Islas, C. A. & Maldonado, P. D. Canonical and non-canonical mechanisms  
480 of Nrf2 activation. *Pharmacol. Res.* **134**, 92–99 (2018).
- 481 37. Lamb, C. A., Yoshimori, T. & Tooze, S. A. The autophagosome: origins unknown,  
482 biogenesis complex. *Nat Rev Mol Cell Biol* **14**, 759–774 (2013).
- 483 38. Mauvezin, C., Ayala, C., Braden, C. R., Kim, J. & Neufeld, T. P. Assays to monitor  
484 autophagy in Drosophila. *Methods* **68**, 134–139 (2014).
- 485 39. Chang, Y.-Y. & Neufeld, T. P. An Atg1/Atg13 complex with multiple roles in TOR-  
486 mediated autophagy regulation. *Mol. Biol. Cell* **20**, 2004–2014 (2009).

- 487 40. Piddini, E., Marshall, F., Dubois, L., Hirst, E. & Vincent, J.-P. Arrow (LRP6) and  
488 Frizzled2 cooperate to degrade Wingless in *Drosophila* imaginal discs.  
489 *Development* **132**, 5479–5489 (2005).
- 490 41. Sancho, M. *et al.* Competitive interactions eliminate unfit embryonic stem cells at  
491 the onset of differentiation. *Dev. Cell* **26**, 19–30 (2013).
- 492 42. Paramore, A. & Frantz, S. Bortezomib. *Nat Rev Drug Discov* **2**, 611–612 (2003).
- 493 43. Pandey, U. B. *et al.* HDAC6 rescues neurodegeneration and provides an  
494 essential link between autophagy and the UPS. *Nature* **447**, 859–863 (2007).
- 495 44. Sung, M.-K., Reitsma, J. M., Sweredoski, M. J., Hess, S. & Deshaies, R. J.  
496 Ribosomal proteins produced in excess are degraded by the ubiquitin-proteasome  
497 system. *Mol. Biol. Cell* **27**, 2642–2652 (2016).
- 498 45. Kraft, C., Deplazes, A., Sohrmann, M. & Peter, M. Mature ribosomes are  
499 selectively degraded upon starvation by an autophagy pathway requiring the  
500 Ubp3p/Bre5p ubiquitin protease. *Nature Publishing Group* **10**, 602–610 (2008).
- 501 46. Wyant, G. A. *et al.* NUFIP1 is a ribosome receptor for starvation-induced  
502 ribophagy. *Science* **360**, 751–758 (2018).
- 503 47. Tye, B. W. *et al.* Proteotoxicity from aberrant ribosome biogenesis compromises  
504 cell fitness. *Elife* **8**, 3429 (2019).
- 505 48. Albert, B. *et al.* A ribosome assembly stress response regulates transcription to  
506 maintain proteome homeostasis. *Elife* **8**, 720 (2019).
- 507 49. Rubinsztein, D. C. The roles of intracellular protein-degradation pathways in  
508 neurodegeneration. *Nature* **443**, 780–786 (2006).
- 509 50. Nezis, I. P. *et al.* Ref(2)P, the *Drosophila melanogaster* homologue of mammalian  
510 p62, is required for the formation of protein aggregates in adult brain. *J. Cell Biol.*  
511 **180**, 1065–1071 (2008).
- 512 51. Cullinan, S. B. & Diehl, J. A. PERK-dependent activation of Nrf2 contributes to  
513 redox homeostasis and cell survival following endoplasmic reticulum stress. *J.*  
514 *Biol. Chem.* **279**, 20108–20117 (2004).
- 515 52. Bjedov, I. *et al.* Mechanisms of Life Span Extension by Rapamycin in the Fruit Fly  
516 *Drosophila melanogaster*. *Cell Metabolism* **11**, 35–46 (2010).
- 517 53. Li, J., Kim, S. G. & Blenis, J. Rapamycin: one drug, many effects. *Cell Metabolism*  
518 **19**, 373–379 (2014).
- 519 54. Laplante, M. & Sabatini, D. M. mTOR Signaling. *Cold Spring Harbor Perspectives*  
520 *in Biology* **4**, (2012).
- 521 55. Webb, A. E. & Brunet, A. FOXO transcription factors: key regulators of cellular  
522 quality control. *Trends in Biochemical Sciences* (2014).  
523 doi:10.1016/j.tibs.2014.02.003
- 524 56. Klockgether, T., Mariotti, C. & Paulson, H. L. Spinocerebellar ataxia. *Nat Rev Dis*  
525 *Primers* **5**, 24–21 (2019).
- 526 57. Bonini, N. M. A genetic model for human polyglutamine-repeat disease in  
527 *Drosophila melanogaster*. *Philos. Trans. R. Soc. Lond., B, Biol. Sci.* **354**, 1057–  
528 1060 (1999).
- 529 58. Recasens-Alvarez, C., Alexandre, C., Kirkpatrick, J., Nojima, H., Huels, D. J.,  
530 Snijders, A. P., & Vincent, J.-P. Ribosomopathy-associated mutations cause  
531 proteotoxic stress that is alleviated by TOR inhibition. *Nature Cell Biology* (2020).

- 532 59. Coelho, D. S. *et al.* Culling Less Fit Neurons Protects against Amyloid- $\beta$ -Induced  
533 Brain Damage and Cognitive and Motor Decline. *CellReports* **25**, 3661–3673.e3  
534 (2018).
- 535 60. Guang, M. H. Z. *et al.* Targeting Proteotoxic Stress in Cancer: A Review of the  
536 Role that Protein Quality Control Pathways Play in Oncogenesis. *Cancers* **11**, 66  
537 (2019).
- 538 61. Jarosz, D. F., Taipale, M. & Lindquist, S. Protein homeostasis and the phenotypic  
539 manifestation of genetic diversity: principles and mechanisms. *Annu. Rev. Genet.*  
540 **44**, 189–216 (2010).
- 541 62. Kaushik, S. & Cuervo, A. M. Proteostasis and aging. *Nat Med* **21**, 1406–1415  
542 (2015).
- 543 63. Taylor, R. C. & Dillin, A. Aging as an Event of Proteostasis Collapse. *Cold Spring*  
544 *Harbor Perspectives in Biology* **3**, a004440–a004440 (2011).

### Figure Legends

548

#### 549 **Figure 1. Reduced protein synthesis does not confer the loser status.**

550 (a-b) Apoptosis detection by cleaved caspase-3 staining (red) in wild type or *RpS3*<sup>+/-</sup>  
551 non-competing (homotypic) wing discs (a) and corresponding quantification (n=7 and  
552 10, respectively, two-sided Mann-Whitney U Test) (b). (c-d) Apoptosis detection by dcp-  
553 1 staining (red) in competing wing discs containing *RpS3*<sup>+/-</sup> cells (GFP-positive) and  
554 unlabeled wild type cells (GFP-negative) (c) and corresponding quantification (n=8, two-  
555 sided Wilcoxon signed-rank test) (d). (e-g) Translation rate measurement by OPP in  
556 wing discs containing wild-type cells and *RpS3*<sup>+/-</sup> clones (GFP-positive) (e) or 4E-BP<sup>TA</sup>-  
557 expressing clones (GFP-positive) (f). Corresponding quantifications are in (g) (n=10 and  
558 10 respectively, two-sided two sample Kolmogorov-Smirnov test). (h-i) Apoptosis  
559 detection by cleaved caspase-3 staining (red) in wing discs with mosaic expression of  
560 4E-BP<sup>TA</sup> (GFP-positive) (h), and corresponding cell death quantifications (n=9, two-  
561 sided Wilcoxon signed-rank test) (i). (j) Wing disc harboring an *RpS3*<sup>+/-</sup> Anterior (A) and  
562 a wild-type Posterior (P) compartments stained for anti-active phospho-JNK (p-JNK,  
563 red). (k) Wing disc expressing 4E-BP<sup>TA</sup> in P compartment stained for p-JNK (red). (l-n)  
564 *GstD1*-GFP signal (green) in wing discs harboring *RpS3*<sup>+/-</sup> A cells (dsRed-positive) and  
565 wild-type P cells (dsRed-negative) (l) and in wing discs harboring 4E-BP<sup>TA</sup>-expressing P  
566 and wild-type A cells (m), and corresponding quantification (n=12 and 10 respectively,  
567 two-sided two sample Kolmogorov-Smirnov test) (n). (o-p) An *RpS3*<sup>+/-</sup> wing disc over-

568 expressing GADD34 in P cells and labelled with OPP (o), and corresponding  
569 quantification (n=5, two-sided paired t-test) (p). (q-s) Wing discs harboring wild-type  
570 cells and *RpS3*<sup>+/-</sup> clones (GFP-positive) (q) or *RpS3*<sup>+/-</sup> clones expressing GADD34  
571 (GFP-positive) (r), and corresponding quantification (n=17 and 10 respectively, two-  
572 sided Mann-Whitney U test) (s). In this figure, for all micrographs, scale bars  
573 correspond to 50µm. All n numbers refer to the number of individual wing discs. In this  
574 figure and throughout: dashed lines indicate wing pouch or clonal and compartment  
575 boundaries; clone border defines cells within 2-cell diameters of the clone perimeter;  
576 Posterior is right and dorsal is up; figure panel genotypes are provided for all figures in  
577 Supplementary Table 3; each point in graphs represents one wing disc, unless  
578 otherwise indicated. For all quantifications, the horizontal line represents the mean and  
579 whiskers indicate 95% confidence intervals.

580  
581  
582

583 **Figure 2. Prospective losers display defective autophagic flux.**

584 (a-b) Apoptotic cell death, as detected by anti-cleaved Caspase-3 reactivity (green), in  
585 wing discs of a *p62*<sup>+/-</sup> heterozygote (a, left), *RpS3*<sup>+/-</sup> heterozygote (a, middle), or *p62*<sup>+/-</sup>,  
586 *RpS3*<sup>+/-</sup> transheterozygote (a, right) and corresponding quantification (n=10, 7, and 11  
587 respectively, two-sided Mann-Whitney U test without p-adjustment for multiple  
588 comparisons) (b). (c) Staining of autophagosomes and autolysosomes, as detected by  
589 atg8-GFP-mCherry expression (red) in the P-compartment of wild type (c, left), or  
590 *Rps3*<sup>+/-</sup> (c, right) wing discs. (d-e) Immunostaining for p62 in wing discs harboring  
591 *RpS3*<sup>+/-</sup> A cells and wild type P cells (d) and corresponding fluorescence intensity  
592 quantification (n=9, two-sided paired t-test) (e). (f) Immunostaining of p62 in a wing disc  
593 with *mahj*<sup>-/-</sup> clones (GFP-negative) induced in a *mahj*<sup>+/-</sup> heterozygous background  
594 (1XGFP). Wild-type twin spots are 2XGFP. (g) Immunostaining for p62 in wing discs  
595 harboring wild-type A cells and 4E-BP<sup>TA</sup>-expressing P cells (labelled by the absence of  
596 Ci, magenta). (h) Schematic representation of ReFLUX: the autophagy cargo p62 is  
597 fused to GFP and driven by a *hs* promoter for pulse-chase expression. (i-k) GFP-p62  
598 ReFlux signal (green) in wing discs harboring *RpS3*<sup>+/-</sup> A cells (dsRed-positive) and wild-  
599 type P cells (dsRed-negative) immediately after heat shock (i), or three hours later (j)

600 and corresponding signal quantifications (n= 7 and 8 respectively, two-sided student's t-  
601 test) (k). (l-n) GFP-p62 ReFlux signal (green) in wing discs expressing *mahj*-RNAi in the  
602 P compartment (RFP-positive), immediately after heat shock (l) or three hours later (m)  
603 and corresponding signal quantifications (n=8 and 7 respectively, two-sided student's t-  
604 test) (n). For all micrographs, scale bars correspond to 50µm. For all quantification, the  
605 horizontal line represents the mean and whiskers indicate 95% confidence intervals. All  
606 n numbers refer to the number of individual wing discs.

607

608 **Figure 3. Autophagy impairment does not confer the loser status.** (a-b) Apoptosis  
609 detection by cleaved caspase-3 staining (red) in wing discs with mosaic expression of  
610 *atg1*-RNAi (GFP-positive cells) (a) and corresponding quantifications (n=9, two-sided  
611 Wilcoxon signed-rank test) (b). Cell death is classed as border death or center death, as  
612 described in Figure 1. (c) p62 staining in wing discs of the same genotype as in (a). (d)  
613 p62 staining (left) and *GstD1*-GFP signal (right) in wing discs harboring *atg1*-RNAi  
614 expressing P cells and wild-type A cells. (e-h) p62 staining (e) and apoptosis detection  
615 by cleaved caspase-3 staining (red) (f) in wing discs with *atg13*<sup>-/-</sup> clones (GFP-negative)  
616 induced in an *atg13*<sup>+/-</sup> heterozygous background (1XGFP), and corresponding cell death  
617 (g, n=12, two-sided Wilcoxon signed-rank test) and clone size (h, n=95 and 105,  
618 respectively, two-sided Mann-Whitney U test) quantifications for *atg13*<sup>-/-</sup> clones and wild-  
619 type *atg13*<sup>+/+</sup> twin spots (2XGFP). Each dot or square on the graph in (h) represents  
620 one clone, and the horizontal line represents the median and whiskers indicate the 95%  
621 confidence interval. (i-k) Wing discs harboring GFP-positive clones expressing *atg9*-  
622 *RNAi* (j) or expressing *atg9*-*RNAi* and 4E-BP<sup>TA</sup> (k) and stained for cleaved-dcp1 (red)  
623 and corresponding cell death quantification in clone centers (Cent.) versus borders  
624 (Bord.) (n=11 and 14 respectively, two-sided Wilcoxon signed-rank test) (i). For all  
625 micrographs, scale bars correspond to 50µm. For all quantifications provided other than  
626 (h), the horizontal line represents the mean and whiskers indicate 95% confidence  
627 intervals. All n numbers refer to the number of individual wing discs, except in (h)  
628 wherein n numbers refer to the number of individual twin-spot clones.

629

630

631 **Figure 4. Prospective losers display proteotoxic stress.** (a-b) Apoptosis detection  
632 by cleaved caspase-3 staining (red) in wild type (a) or *RpS3<sup>+/-</sup>* (b) wing discs fed DMSO  
633 or 10  $\mu$ M bortezomib, as indicated. (c) Quantification of dying cell numbers within the  
634 pouch region of wing discs from the conditions indicated in (a-b) (n=8, 8, 7, and 5,  
635 respectively, two-sided Mann-Whitney U test without p-adjustment for multiple  
636 comparisons). (d) Schematic representation of ProteoFLUX: a fusion of GFP with the  
637 proteasome degradation signal CL1, driven by a *hs* promoter for pulse-chase  
638 expression. (e-f) ProteoFLUX CL1-GFP signal (green) in wing discs expressing RNAi  
639 against the proteasomal subunit *Rpt6* specifically in P cells, immediately after heat  
640 shock or two hours later, as indicated (e), and corresponding signal quantifications (n=3  
641 and 11 respectively, two-sided Mann-Whitney U test) (f). (g-i) ProteoFLUX CL1-GFP  
642 signal (green) in wing discs harboring *RpS3<sup>+/-</sup>* A cells (dsRed-positive) and wild-type P  
643 cells (dsRed-negative), immediately after heat shock (g), or two hours later (h), and  
644 corresponding signal quantifications (n=7 and 7 respectively, two-sided student's t-test)  
645 (i). (j) Abundance of Ribosomal subunit proteins in *RpS3<sup>+/-</sup>* wing discs relative to wild-  
646 type wing discs by TMT Mass Spectrometry. Bars indicate average log fold change  
647 values across two independent biological replicates. (k) Proteostat protein aggregate  
648 staining (green) in wing discs harboring *RpS3<sup>+/-</sup>* A cells and wild-type P cells. (l) FK2  
649 anti-conjugated ubiquitin (green) and anti-p62 (red) staining in a wing disc harboring an  
650 *RpS3<sup>+/-</sup>* A compartment and a wild-type P compartment, as indicated. Yellow boxes  
651 mark inset locations. For all micrographs, scale bars correspond to 50 $\mu$ m. For all  
652 quantifications provided, the horizontal line represents the mean and whiskers indicate  
653 95% confidence intervals. All n numbers refer to the number of individual wing discs.

654  
655 **Figure 5. Alleviating proteotoxic stress rescues the loser status.** (a-b) Apoptosis  
656 detection by cleaved caspase-3 staining (red) in competing wing discs containing  
657 *RpS3<sup>+/-</sup>* cells (GFP-positive) and unlabeled wild type cells (GFP-negative) from larvae  
658 fed ethanol carrier (a) or 4  $\mu$ M rapamycin (b). (c) Quantification of cell death at *RpS3<sup>+/-</sup>*  
659 clone boundaries for the experiments in (a-b) (n=13 and 12 respectively, two-sided two  
660 sample Kolmogorov-Smirnov test). (d-e) *GstD1*-GFP signal (green) in *RpS3<sup>+/-</sup>* wing discs  
661 fed EtOH control or 4 $\mu$ M Rapamycin, as indicated (d), and corresponding quantification

662 (n=10 and 12 respectively, two-sided student's t-test) (e). (f) p62 staining in *RpS3*<sup>+/-</sup>  
663 wing discs expressing FOXO in P cells (labelled by the absence of Ci, magenta). (g-h)  
664 An *RpS3*<sup>+/-</sup> wing disc harboring FOXO expressing clones (GFP-positive) and labelled  
665 with OPP (red) (g) with corresponding quantification in (h) (n=8, two-sided paired t-test).  
666 (i-j) Phospho-eIF2 $\alpha$  staining (red) in *RpS3*<sup>+/-</sup> wing discs expressing FOXO in P cells (i)  
667 and corresponding quantification (n=10, two-sided Wilcoxon signed-rank test. Due to  
668 low genetic frequency and the presence of an internal control, samples from multiple  
669 experiments were pooled together) (j). (k-l) Apoptosis detection by cleaved caspase-3  
670 staining (red) in competing wild-type/*RpS3*<sup>+/-</sup> mosaic wing discs without (k) or with (l)  
671 additional expression of dFOXO specifically in *RpS3*<sup>+/-</sup> cells. (m) Quantification of cell  
672 death at *RpS3*<sup>+/-</sup> clone boundaries for the experiments in (k-l) (n=8 and 10, respectively,  
673 two-sided two sample Kolmogorov-Smirnov test). For all micrographs, scale bars  
674 correspond to 50 $\mu$ m. For all quantifications provided, the horizontal line represents the  
675 mean and whiskers indicate 95% confidence intervals. All n numbers refer to the  
676 number of individual wing discs.

677

678 **Figure 6: Proteotoxic stress is sufficient to confer the loser status.** (a-b) *GstD1*-  
679 GFP signal (green) in a wing disc expressing MJDQ78 in P cells (labelled by the  
680 absence of Ci, magenta) (a) and corresponding quantification (n=8, two-sided Wilcoxon  
681 signed-rank test) (b). (c) GFP-p62 ReFlux signal (green) in wing discs expressing  
682 MJDQ78 in P cells, immediately after heat shock or three hours later, as indicated. (d-e)  
683 p62 staining in a wing disc expressing MJDQ78 in P cells (labelled by the absence of  
684 Ci, magenta) (d), and corresponding quantification in (e) (n=7, two-sided paired t-test).  
685 (f-g) Wing discs harboring GFP-positive clones expressing MJDQ78 labelled with OPP  
686 (red) (f) with corresponding quantification relative to wing discs containing competing  
687 *RpS3*<sup>+/-</sup> clones and wildtype winners (image not shown) in (g) (n=6 and 7 respectively,  
688 two-sided student's t-test). (h-i) Mosaic wing disc containing GFP-positive clones  
689 overexpressing MJDQ78, immuno-stained for cleaved Caspase-3 (red) (h), and  
690 corresponding cell death quantification (n= 11, two-sided Wilcoxon signed-rank test) (i).  
691 (j-l) Wing discs harboring wild-type cells and wildtype control clones (GFP-positive) (k)  
692 or clones expressing MJDQ78 (GFP-positive) (l), and corresponding quantification



693 (n=15 and 20 respectively, two-sided Mann-Whitney U test) (**j**). (**m**) Model summarizing  
694 how ribosome gene loss leads to proteotoxic stress and to the loser status. For all  
695 micrographs, scale bars correspond to 50µm. For all quantifications provided, the  
696 horizontal line represents the mean and whiskers indicate 95% confidence intervals. All  
697 n numbers refer to the number of individual wing discs.

698

699

1  
2  
3  
4  
5  
6  
7  
8  
9

## **Methods**

### **Proteotoxic stress is a driver of the loser status and of cell competition**

Michael E. Baumgartner, Michael P. Dinan, Paul F. Langton, Iwo Kucinski, and Eugenia Piddini

10

11 **Fly husbandry.** Fly lines were maintained at 25°C on a flour-based food supplemented  
12 with yeast. Our standard recipe contains 7.5g/L agar powder, 50g/L baker's yeast,  
13 55g/L glucose, 35g/L wheat flour, 2.5 % nipagin, 0.4 % propionic acid and 1.0%  
14 penicillin/streptomycin. For some chemical feeding experiments, drugs were diluted in  
15 Nutrifly GF food (Scientific Laboratory Supplies) made to manufacturer's instructions.  
16 Sexes were not differentiated for any experiments, except in cases where transgenes  
17 were X-linked. Eggs were collected for 24 hours and wing discs were dissected from  
18 wandering third instar larvae. For each dataset, including across different vials or  
19 genotypes, egg collections, heat-shocks and harvesting of wandering stage larvae for  
20 dissections were done in parallel. All *Drosophila* strains used in this study are provided  
21 in Supplemental Table 2, and genotypes for all experimental crosses are provided in  
22 Supplemental Table 3.

23

24 **Immunostaining.** Wing discs were dissected in phosphate-buffered saline (PBS)  
25 before fixation in 4% formaldehyde/PBS solution for 20 minutes at room temperature.  
26 Dissected hemi-larvae were subsequently washed three times in PBS (30 seconds  
27 each), before permeabilisation in PBS containing 0.25% Triton X-100 (PBS-T). Samples  
28 were next incubated in blocking buffer (PBS-T supplemented with 4% fetal calf serum)  
29 for 30 minutes at room temperature. Primary antibodies were diluted in blocking buffer  
30 and incubated overnight at 4°C. Samples were washed three times in PBS-T (10  
31 minutes each) before incubation in secondary antibody (diluted in blocking buffer) for 1  
32 hour at room temperature. The secondary antibodies used were conjugated with Alexa  
33 488, Alexa 555 or Alexa 633 dyes (Molecular probes). Nuclei were counterstained with  
34 DAPI (0.5 µg/ml). After three 5-minute washes in PBS-T, wing discs were mounted in  
35 Vectashield (Vector laboratories) on a borosilicate glass slide (no 1.5, VWR  
36 international). For anti-FK-2 staining, the blocking buffer was substituted with a 3% BSA  
37 in PBS solution. Details and sources of all antibodies are provided in Supplemental  
38 Table 2. Dilutions for primary antibodies used are as follows: 1 in 500 for anti-pJNK, 1 in  
39 1000 for anti-Ci, 1 in 2000 for anti-Ref(2)P, 1:25000 for anti-cleaved Caspase-3, 1 in  
40 2500 for anti-DCP1, 1 in 500 for anti-p-eIF2α, and 1 in 5000 for anti-FK2.

41

42 **Clonal analysis.** Mosaic wing discs were generated using the FLP/FRT system  
43 employing *hs-FLP* or *en-Gal4-UAS-FLP* transgenic strains. For clone induction, heat  
44 shocks were carried out 2-4 days after egg laying (depending on experiment), in a 37°C  
45 water bath before returning flies to a 25°C incubator, or for experiments employing a  
46 temperature sensitive Gal80 (Gal80<sup>TS</sup>), to a water bath at the indicated temperature.  
47 The exact temperature for Gal80<sup>TS</sup> experiments together with heat shock conditions  
48 and clone age, which were optimized for each experiment individually, are listed in  
49 Supplemental Table 3.

50

51 **Translation Assays.** AHA and OPP assays were carried out using the Click-iT™ Plus  
52 OPP Protein Synthesis Assay kit and Click-iT Plus™ AHA Protein Synthesis Assay kit,  
53 respectively. For the AHA assay, wing discs were dissected and inverted in a glass dish  
54 before incubation in methionine free Schneider's medium at 25 °C for 45 min. Hemi-  
55 larvae were then incubated for a further 45 min in methionine free medium  
56 supplemented with 2 mM AHA reagent. Samples were subsequently washed in PBS  
57 before fixation in 4% formaldehyde/PBS solution. For OPP assays, larvae were  
58 dissected in normal Schneider's medium before transfer to a 1.5 ml Eppendorf  
59 containing 5 μM OPP reagent in Schneider's medium and incubation for 15 min at 25  
60 °C. Samples were subsequently washed in PBS before fixation. For both assays, fixed  
61 tissues were subsequently stained using the standard Click-iT protocol according to  
62 manufacturer's instructions. Details for reagents are provided in Supplemental Table 2.

63

64 **Identification of proteostasis genes.** The full list of genes differentially expressed in  
65 *RpS3<sup>+/-</sup>* cells plus/minus expression of the JNK inhibitor *puc* was reported previously<sup>20</sup>.  
66 To identify differentially expressed proteostasis genes from this list we selected genes  
67 associated with the following GO terms: autophagy, response to unfolded proteins,  
68 proteasome complex, proteasome catabolic process.

69

70 **Re-Flux and Proteo-Flux Assays.** Re-Flux and Proteo-Flux assays were carried out as  
71 pulse-chase experiments. Third instar wandering larvae were heat-shocked for 40 to 45

72 minutes, to induce a pulse of GFP-p62 or CL1-GFP, respectively. Larvae were  
73 incubated at 25 degrees for the indicated times to chase protein levels before  
74 dissection.

75

76 **Proteostat assay.** For PROTEOSTAT® Protein Aggregation Assay larvae were  
77 dissected and inverted in PBS before transfer to a 1.5 ml Eppendorf tube containing 4%  
78 formaldehyde diluted in 1X PROTEOSTAT assay buffer (PAB). The samples were  
79 subsequently permeabilized in 0.5% Triton X-100, 3 mM EDTA, pH 8.0 diluted in 1X  
80 PAB, before staining with PROTEOSTAT detection reagent diluted 1 in 20,000 together  
81 with Hoechst 33342 at 1 µg/ml in PAB. Hemi-larvae were subsequently washed three  
82 times in PBS before separating wing discs from the larval body and mounting in PBS  
83 under our standard cover slips. Wing discs were imaged immediately. Details for  
84 reagents are provided in Supplemental Table 2.

85

86 **Transmission electron microscopy.** Larvae were washed and dissected in  
87 Schneider's Insect Medium and imaginal wing discs were dissected out and subjected  
88 to high-pressure freezing in a 20% BSA solution followed by an osmium tetroxide freeze  
89 substitution and Epon embedding. The resulting blocks were sectioned onto grids using  
90 an ultramicrotome and stained with uranyl acetate and lead citrate. Sections were then  
91 imaged on a Tecnai 12 transmission electron microscope.

92

93 **Chemical feeding.** For bortezomib feeding, eggs were collected for 24 hours and  
94 larvae grown on normal food for 72 hours before being floated in a 20% sucrose  
95 solution. Floated larvae were thoroughly washed with PBS before transferring to Nutri-  
96 Fly™ GF Premixed food containing 10 µM bortezomib or the equivalent volume of  
97 DMSO (as a carrier control). Larvae were grown until they were at third instar wandering  
98 stages. For rapamycin feeding, 4 µM rapamycin was diluted in standard wheat-based  
99 food and floated larvae were maintained on the drug (or equivalent carrier control of  
100 ethanol) until wandering stage. For chloroquine incubation, dissected larvae were  
101 incubated in 50 µM chloroquine diluted in normal Schneider's medium (or the equivalent

102 volume of water as a carrier control) for three hours at 25 °C, before washing in PBS  
103 and fixation. Details for reagents are provided in Supplemental Table 2.

104

105 **Proteomics.** Third instar larvae raised on normal food were dissected in ice-cold PBS  
106 containing 1X Phos-STOP phosphatase inhibitor and 1X Halt Protease Inhibitor cocktail.  
107 Wing discs were then centrifugated in an Eppendorf containing PBS/inhibitor cocktail for  
108 30 seconds at 6,000 rcf at 4 °C before being lysed in ice-cold RIPA lysis buffer. Lysed  
109 samples were centrifugated at 12,500 rcf at 4 °C for ten minutes. Aliquots of 50µg of  
110 each sample were digested with trypsin (1.25µg trypsin; 37°C, overnight), and labelled  
111 with Tandem Mass Tag (TMT) ten plex reagents according to the manufacturer's  
112 protocol (Thermo Fisher Scientific, Loughborough, LE11 5RG, UK) before samples  
113 were pooled. 40ug of the pooled sample was desalted using a SepPak cartridge  
114 according to the manufacturer's instructions (Waters, Milford, Massachusetts, USA).  
115 Eluate from the SepPak cartridge was evaporated to dryness and resuspended in buffer  
116 A (20 mM ammonium hydroxide, pH 10) prior to fractionation by high pH reversed-  
117 phase chromatography using an Ultimate 3000 liquid chromatography system (Thermo  
118 Fisher Scientific). In brief, the sample was loaded onto an XBridge BEH C18 Column  
119 (130Å, 3.5 µm, 2.1 mm X 150 mm, Waters, UK) in buffer A and peptides eluted with an  
120 increasing gradient of buffer B (20 mM Ammonium Hydroxide in acetonitrile, pH 10)  
121 from 0-95% over 60 minutes. The resulting fractions were evaporated to dryness and  
122 resuspended in 1% formic acid prior to analysis by nano-LC MSMS using an Orbitrap  
123 Fusion Lumos mass spectrometer (Thermo Scientific).

124

125 High pH reversed-phase fractions were further fractionated using an Ultimate 3000  
126 nano-LC system in line with an Orbitrap Fusion Lumos mass spectrometer (Thermo  
127 Scientific). All spectra were acquired using an Orbitrap Fusion Lumos mass  
128 spectrometer controlled by Xcalibur 3.0 software (Thermo Scientific) and operated in  
129 data-dependent acquisition mode using an SPS-MS3 workflow. FTMS1 spectra were  
130 collected at a resolution of 120 000, with an automatic gain control (AGC) target of 400  
131 000 and a max injection time of 100ms. Precursors were filtered with an intensity  
132 threshold of 5000, according to charge state (to include charge states 2-7) and with

133 monoisotopic peak determination set to Peptide. Previously interrogated precursors  
134 were excluded using a dynamic window (60s +/-10ppm). The MS2 precursors were  
135 isolated with a quadrupole isolation window of 0.7m/z. ITMS2 spectra were collected  
136 with an AGC target of 10 000, max injection time of 70ms and CID collision energy of  
137 35%.

138

139 For FTMS3 analysis, the Orbitrap was operated at 30 000 resolution with an AGC target  
140 of 50 000 and a max injection time of 105ms. Precursors were fragmented by high  
141 energy collision dissociation (HCD) at a normalised collision energy of 60% to ensure  
142 maximal TMT reporter ion yield. Synchronous Precursor Selection (SPS) was enabled  
143 to include up to 5 MS2 fragment ions in the FTMS3 scan.

144

145 The raw data files were processed and quantified using Proteome Discoverer software  
146 v2.1 (Thermo Scientific) and searched against the UniProt Drosophila melanogaster  
147 database (downloaded March 2020: 41311 entries) using the SEQUEST HT algorithm.  
148 Peptide precursor mass tolerance was set at 10ppm, and MS/MS tolerance was set at  
149 0.6Da. Searches were performed with full tryptic digestion and a maximum of 2 missed  
150 cleavages were allowed. The reverse database search option was enabled and all data  
151 was filtered to satisfy false discovery rate (FDR) of 5%. Ribosomal proteins were  
152 identified by cross referencing the proteomic results against the 'Ribosomal Protein'  
153 category in FlyBase using R statistical software. Average fold changes were obtained  
154 for Ribosomal Proteins which exhibited a consistent change in relative abundance  
155 across both biological replicates. Two biological replicates were performed.

156

157 **Cloning and transgenics.** To isolate genomic DNA, a single fly was homogenized in  
158 50 µl extraction buffer containing 10 mM Tris HCl pH 8.2, 2 mM EDTA pH 8.0, 0.1%  
159 Triton X-100 and 200 µg/ml proteinase K. Samples were then heated to 55 °C for 30  
160 min in a Thermoshaker with occasional vortexing, before increasing the temperature to  
161 95 °C for 15 min to inhibit protease activity. Samples were then cooled to 4 °C and  
162 centrifuged at 5,000 x g for 5 min at 4 °C. The supernatant was subsequently  
163 transferred to a fresh 0.5 ml Eppendorf tube and stored at 4 °C. Alternatively, DNA was

164 isolated from 10-15 flies using a Gentra Puregene Tissue Kit using the following  
165 protocol: flies were homogenized using a motorized pestle in 200 µl cell lysis buffer and  
166 incubated at 65 °C in a Thermoshaker for 15 min. Then, 1 µl RNAase A solution was  
167 added, before incubation at 37 °C for a further 15 min. A volume of 100 µl of protein  
168 precipitation buffer was subsequently added and samples were thoroughly mixed and  
169 incubated on ice for 5 min. Samples were centrifuged for 10 min at 4 °C, at max speed  
170 before adding 300 µl isopropanol to the supernatant, mixing well and a further 15 min in  
171 the centrifuge. The resulting pellet was washed twice with 70 % ethanol before re-  
172 suspending in 50 µl of DNase free water.

173  
174 For cloning of both ReFLUX (hs-GFP-p62) and ProteoFLUX (hs-CL1-GFP) constructs,  
175 gDNA was isolated from 10-15 flies of the genotypes *UAS-GFP-p62* or *UAS-CL1-GFP*  
176 respectively. The resulting gDNA was used as template for a PCR using primers  
177 designed to amplify constructs introduced in the common pUAST vector. To generate  
178 pCaSper-hs-GFP-p62 three different pairs of primers were used to generate a PCR  
179 product that could be inserted into the pCR™4-TOPO™ vector. The resulting pTOPO-  
180 GFP-p62 together with pCaSper-hs were digested with XbaI and NotI restriction  
181 enzymes (New England Biosciences Ltd) to produce a fragment containing GFP-p62  
182 that could be ligated into the pCaSper-hs backbone. For the hs-CL1-GFP, a protocol  
183 using Infusion® HD Cloning Plus Kit was designed to infuse a PCR product containing  
184 the CL1-GFP sequencing into the pCasper-hs-GFP-p62 plasmid.

185  
186 For cloning of the *act>RpS3>Gal4* construct, the Infusion® HD Cloning Plus Kit  
187 (Clontech, 638909) was used to linearize an extant pCaSper2-act>CD2>Gal4 vector<sup>64</sup>,  
188 by digestion with the *Acc65I* restriction enzyme (NEB). Two PCR products from a  
189 plasmid encoding *RpS3* together with *Hsp70* terminator sequences, were then infused.  
190 The resulting plasmid was transformed into Stellar™ competent cells (Clontech,  
191 636766).

192



193 Plasmids for all constructs were sent for injection into a *w118* line by Genetics Services,  
194 University of Cambridge or BestGene *Drosophila* embryo injection services. Exact  
195 primers used are provided in Supplemental Table 2.

196

197 **Image acquisition and processing.** Confocal images were acquired using Leica SP5  
198 and SP8 confocal microscopes using a 40x 1.3 NA P Apo Oil objective. All wing discs  
199 were imaged as z-stacks with each section corresponding to 0.5-1  $\mu\text{m}$ . Images were  
200 subsequently analysed and processed using Fiji2 and Photoshop (Adobe Version CS6).  
201 Clonal areas were determined using a custom script built in Fiji. For cell death  
202 quantifications, caspase-3 or DCP1 positive cells were counted in the region specified in  
203 each experiment (as reported in the figure legend). All counts were normalized to their  
204 respective area as measured in Fiji. For signal intensity, mean grey value was  
205 measured in Fiji for the specified genotypes within the pouch region of the wing disc.

206

207 **Quantifications.** For immunofluorescence and fluorescent reporter microscopy-based  
208 assays, all measurements were derived from the pouch region of the wing disc. For cell  
209 death assays, death counts were normalized to the area of the wing pouch or to the  
210 specified region of the clones within the pouch. For all scatter dot plots, unless  
211 otherwise specified, the horizontal line represents the mean and whiskers indicate 95%  
212 confidence intervals.

213

214 **Statistics and reproducibility.** All data used for statistical tests along with the specific  
215 test used for each experiment are shown in the Statistics Source Data table. Statistical  
216 tests were performed using GraphPad Prism 7.0a and Rstudio software. P-values were  
217 determined using univariate statistics. We consider not significant (n.s.) p-values  $>0.05$ .  
218 Parametric tests were used in cases where assumptions of normality and equivalence  
219 of variance were met. Non-parametric tests were used otherwise. The parametric tests  
220 used were Student's T-Test and paired T-Test for matched data. The non-parametric  
221 tests used were either a Kolmogorov-Smirnov test or Mann Whitney U-test, or Wilcoxon  
222 matched-pairs signed rank test for matched data. P-value corrections for multiple  
223 comparisons were not considered due to the low number of comparisons. All statistical

224 tests were two-sided. A minimum of three biological repeats were used for experiments  
225 comparing across separate wing discs. For matched experiments containing an internal  
226 control, a minimum of two biological repeats were performed. Functional validation of  
227 reagents and *Drosophila* stocks (e.g. RNAi) was carried out at least once. All data  
228 points for all replicates for specific quantifications are provided in the 'Statistics Source  
229 Data' supplemental file.

230

231 **Code availability:** The Fiji-based custom-made script can be made available to  
232 individuals upon reasonable request, while we seek to publish it independently of this  
233 study.

234

235 **Data availability:** All source numerical data are provided in the Statistics Source Data  
236 table. All other data supporting the findings of this study are available upon reasonable  
237 request. The following publicly available databases were used in this study: Flybase  
238 (<https://flybase.org>); Uniprot D. melanogaster proteome  
239 (<https://www.uniprot.org/proteomes/UP000000803>).

240

241

242

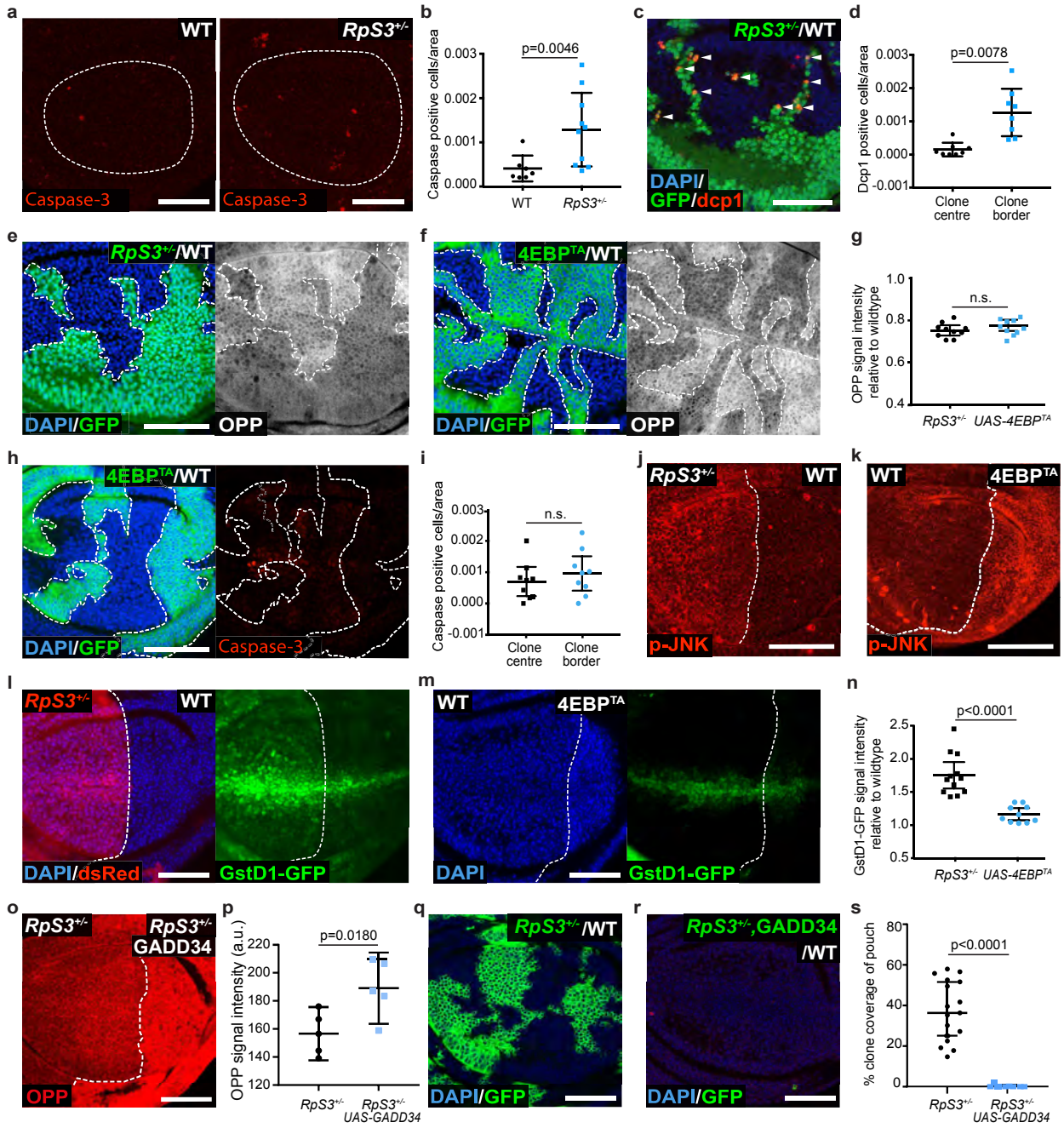
243

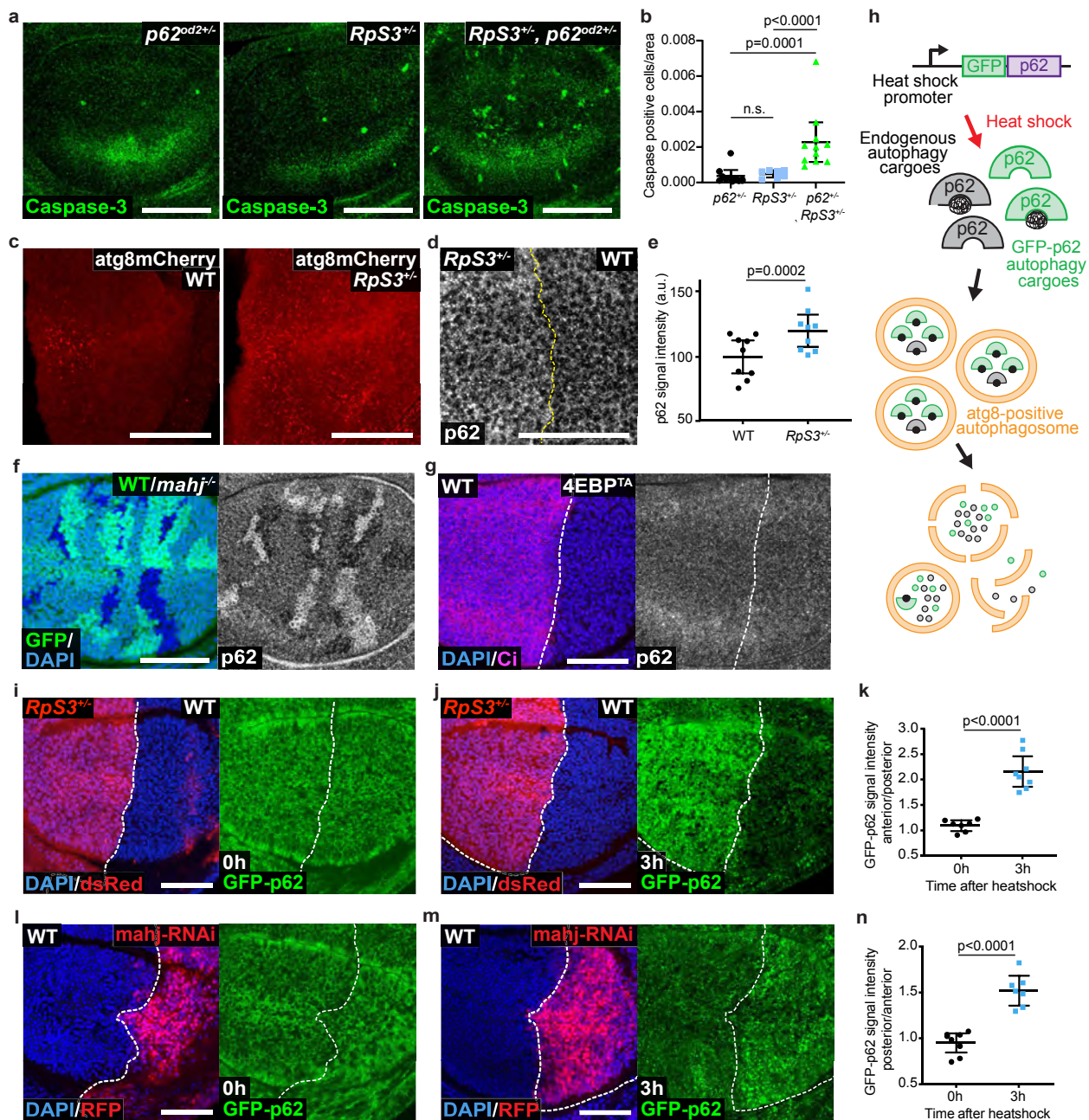
## References

244

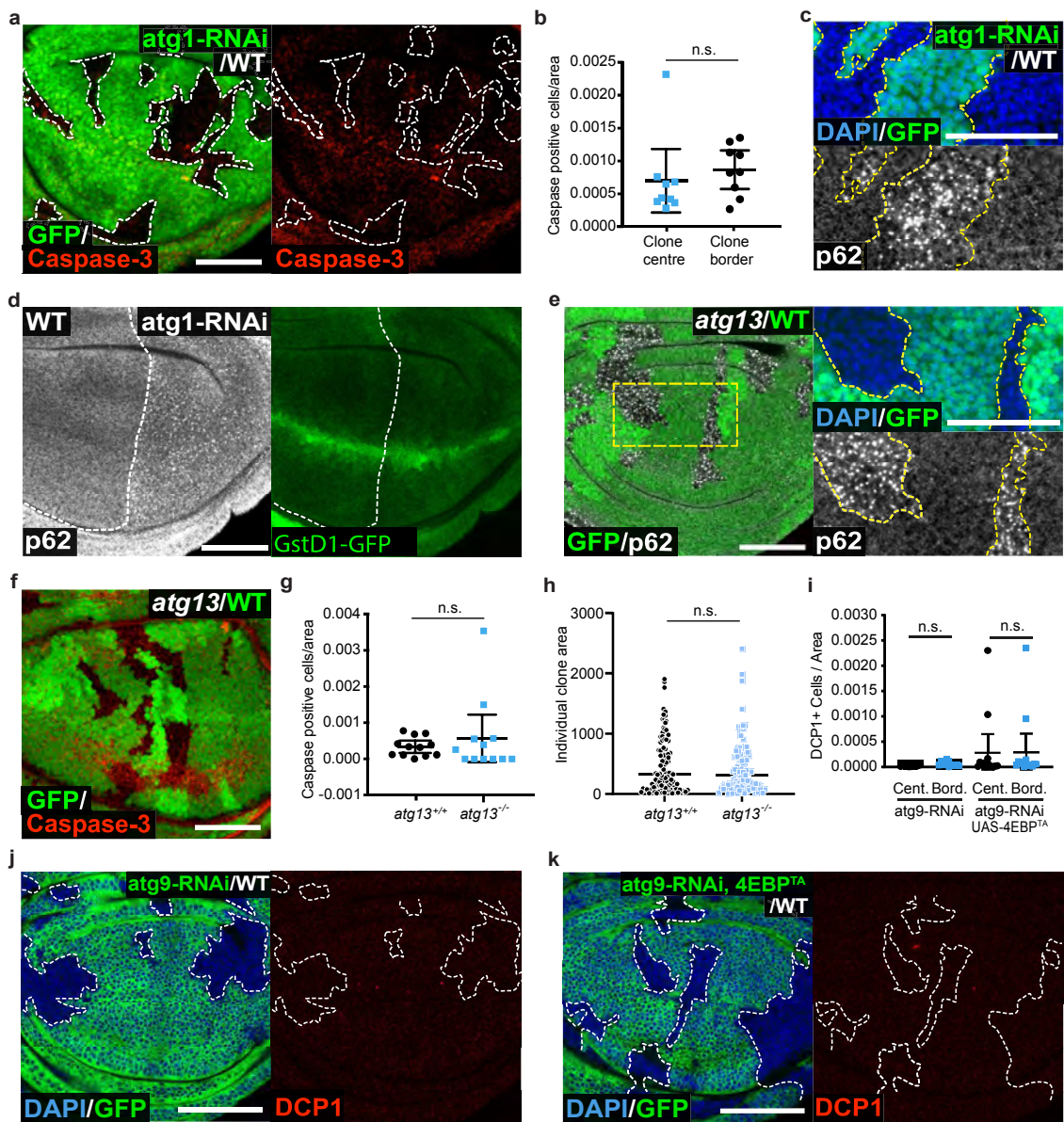
- 245 64. Zhou, Q., Neal, S. J. & Pignoni, F. Mutant analysis by rescue gene excision: New  
246 tools for mosaic studies in *Drosophila*. *Genesis* **54**, 589–592 (2016).
- 247 65. Katheder, N. S. *et al.* Microenvironmental autophagy promotes tumour growth.  
248 *Nature* **541**, 417–420 (2017).
- 249 66. Gay, P. & Contamine, D. Study of the ref(2)P locus of *Drosophila melanogaster*.  
250 II. Genetic studies of the 37DF region. *Mol. Gen. Genet.* **239**, 361–370 (1993).

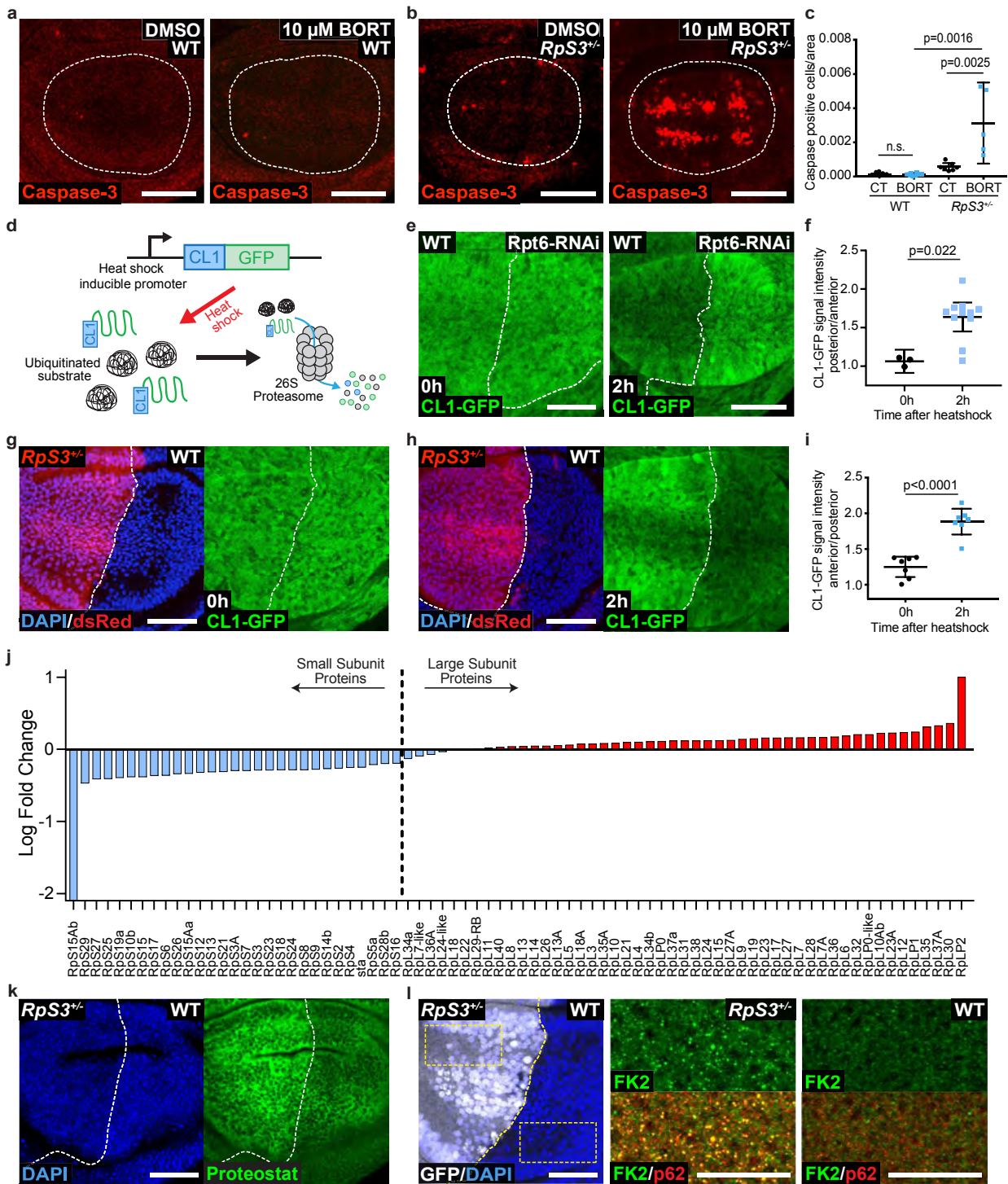
251

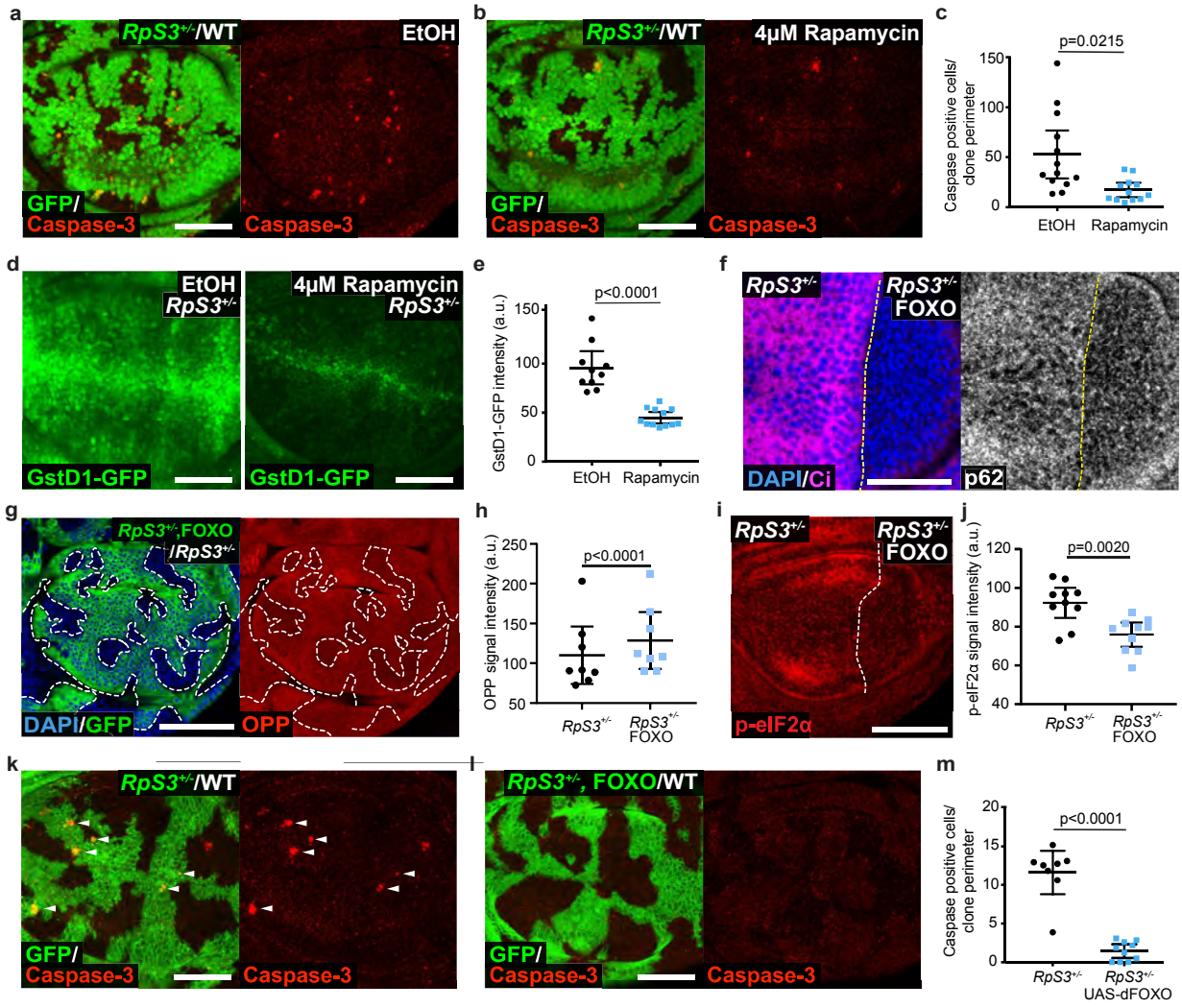




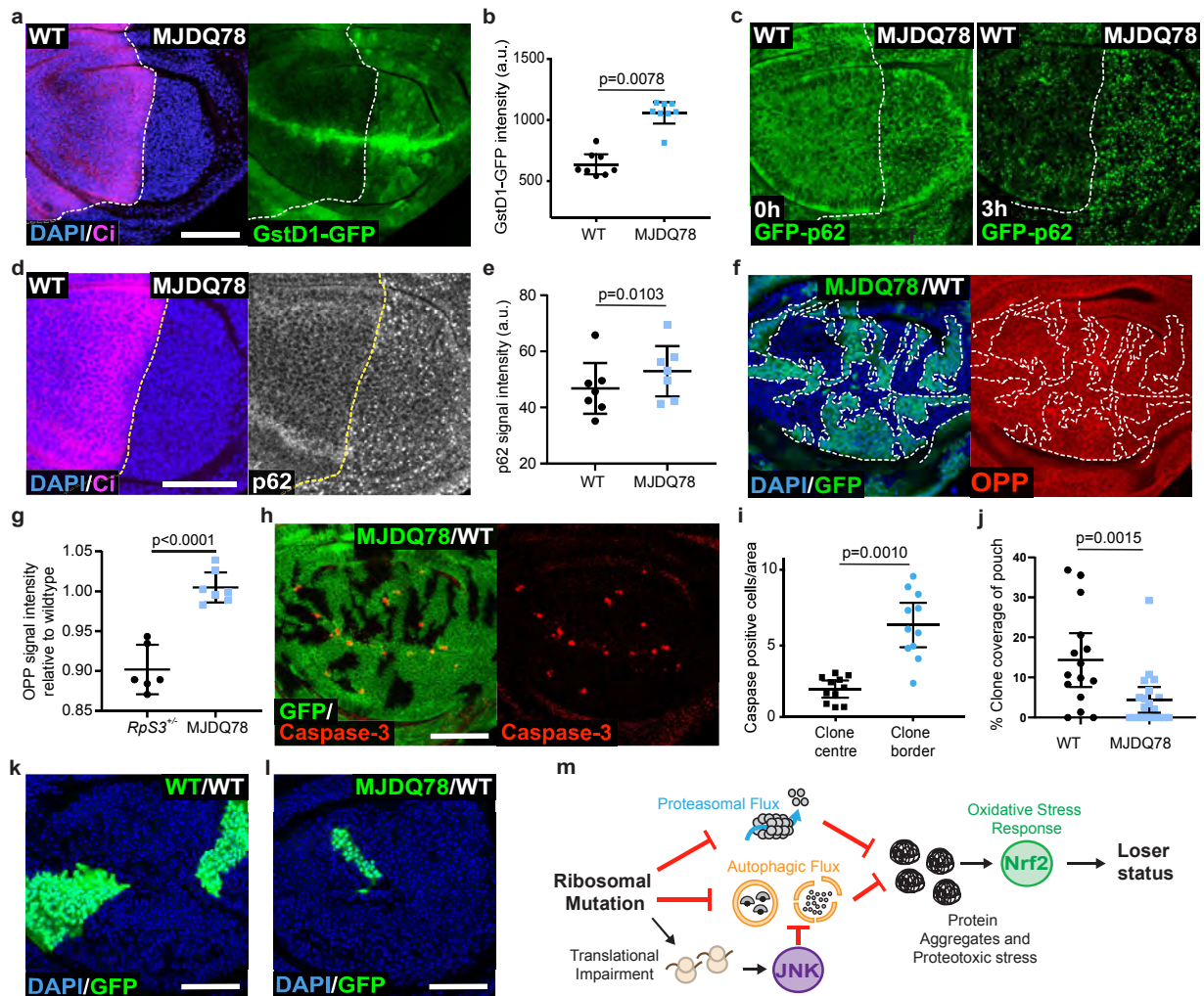




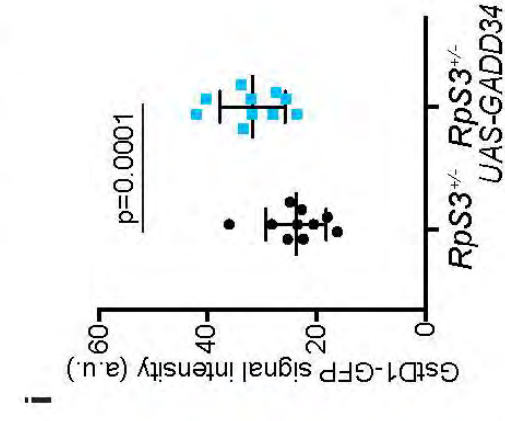
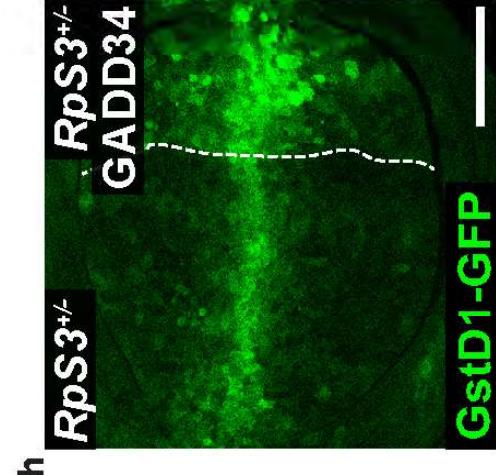
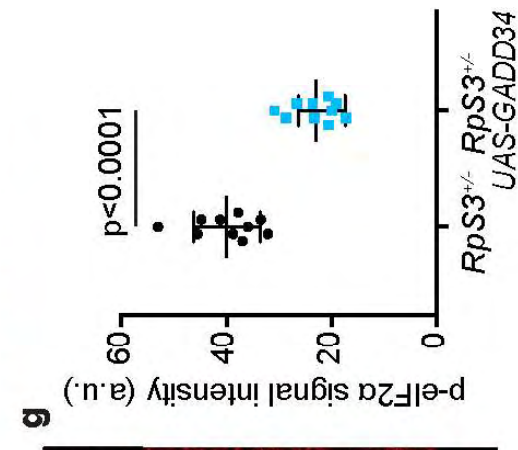
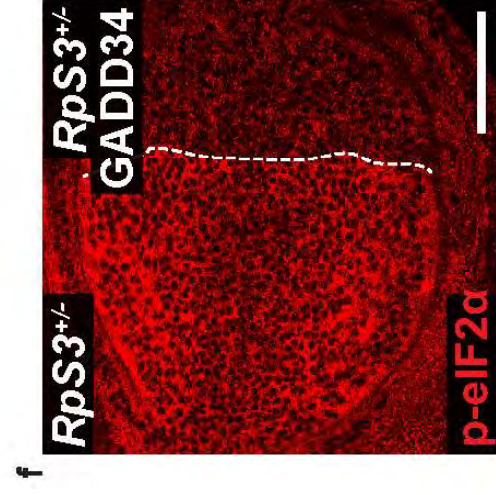
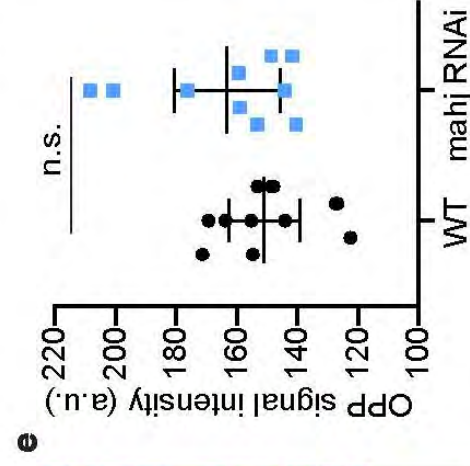
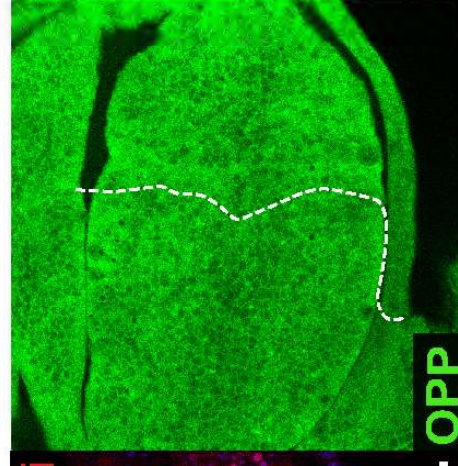
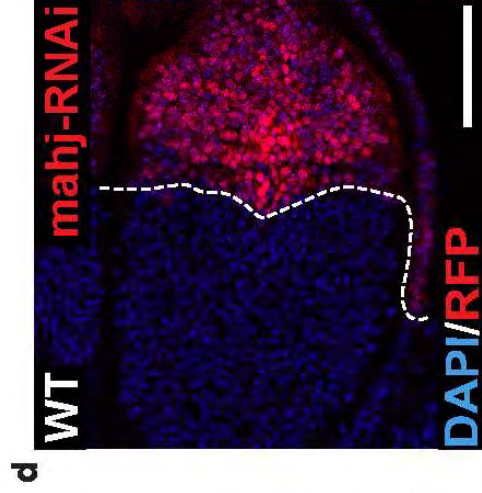
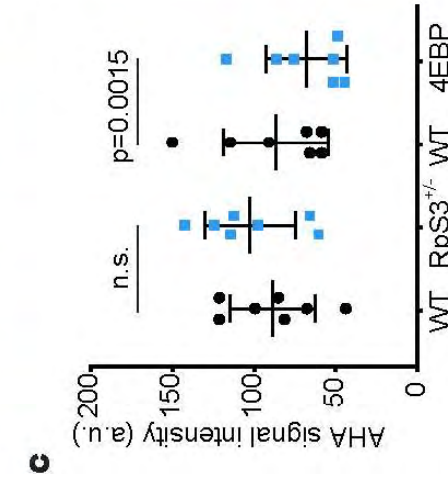
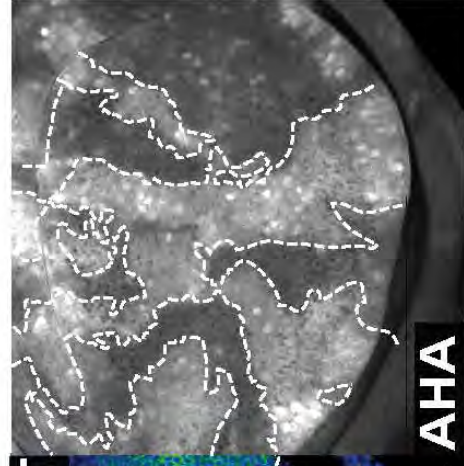
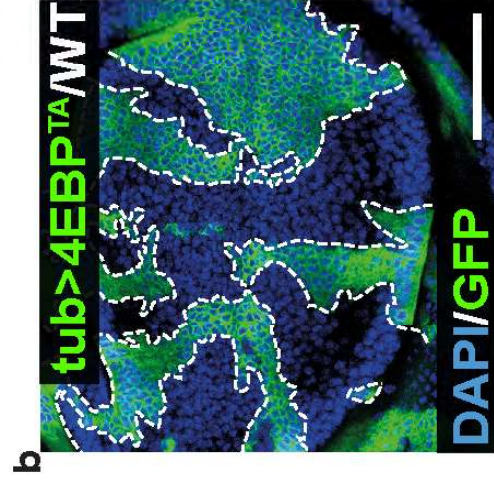
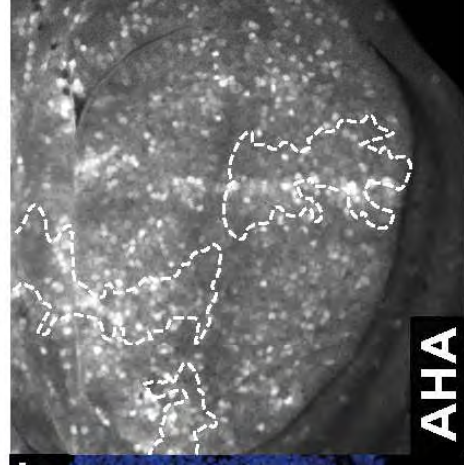
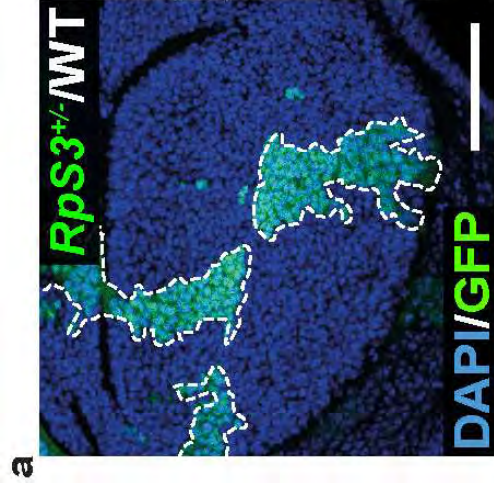




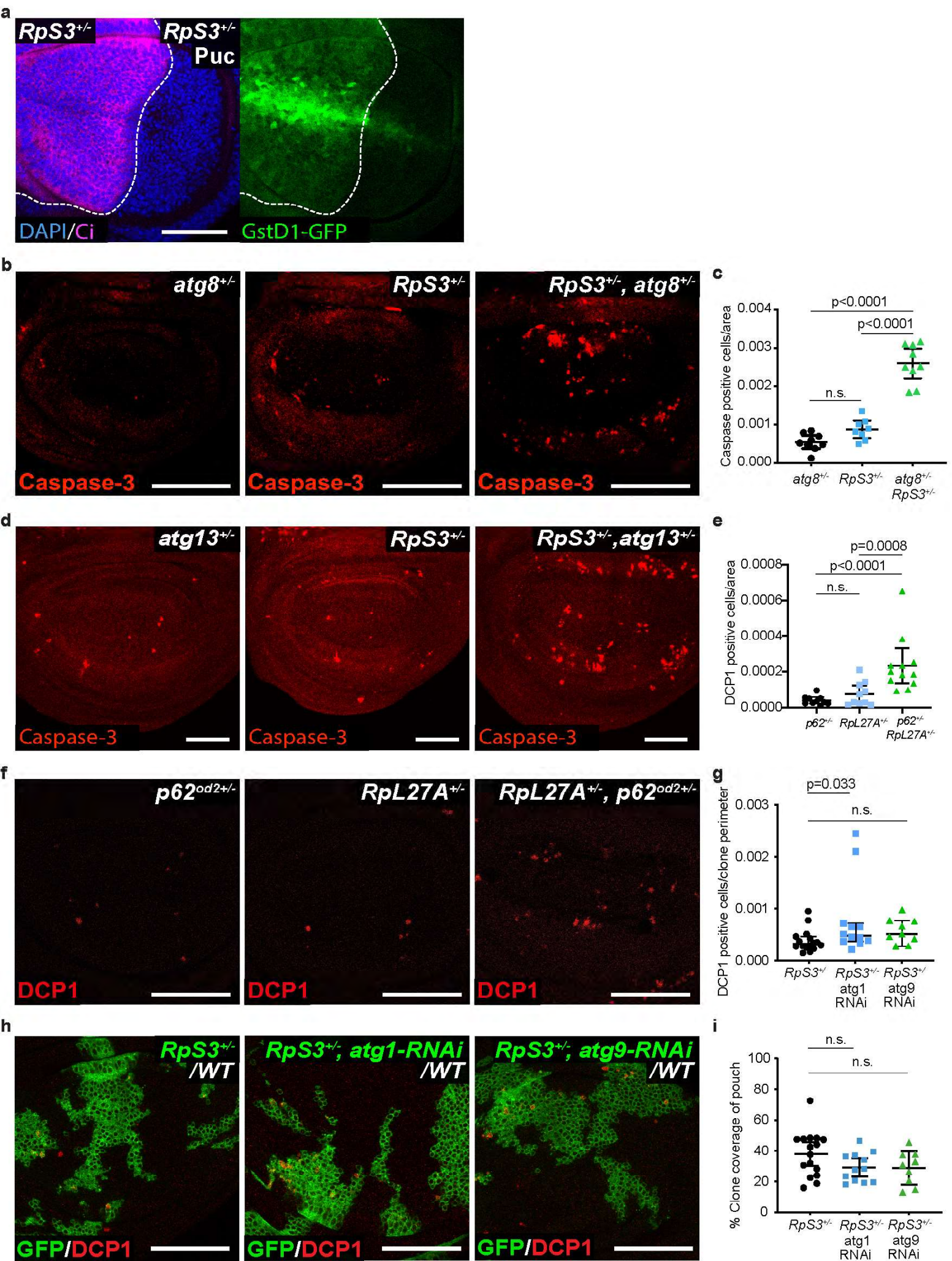




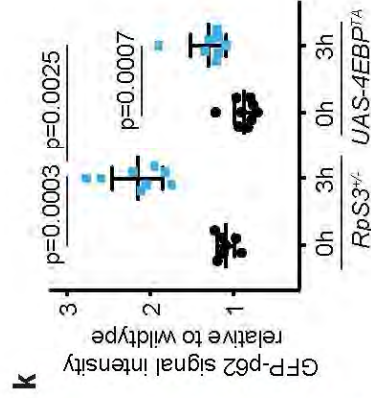
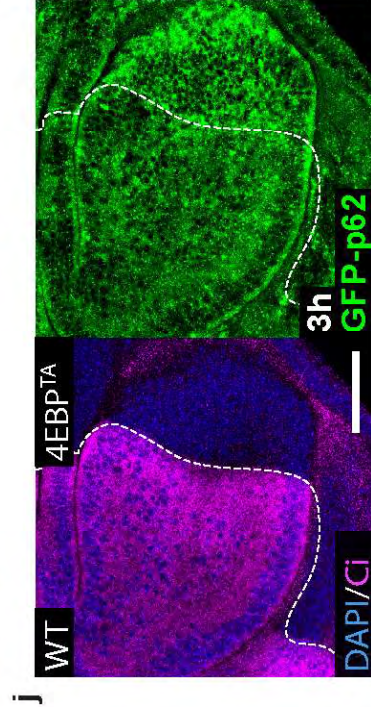
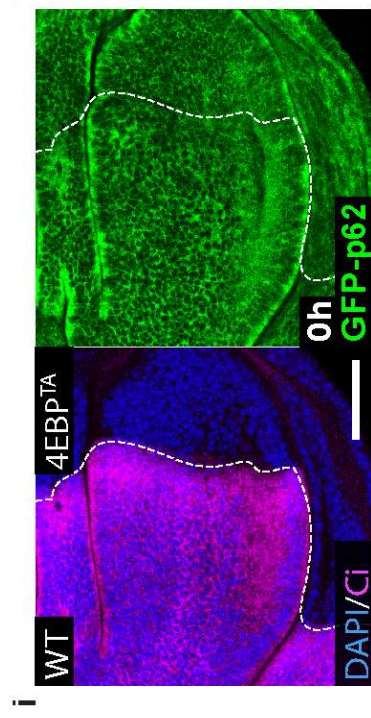
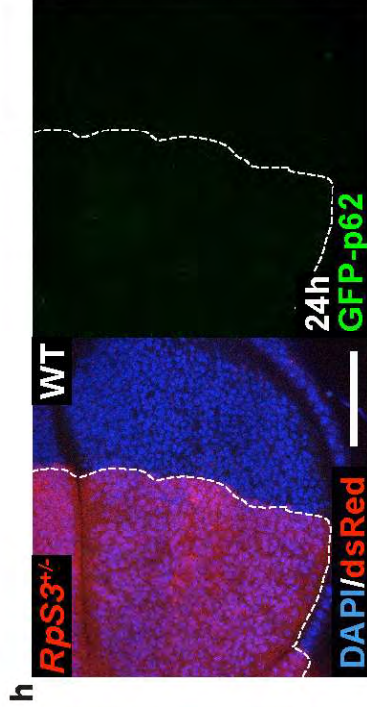
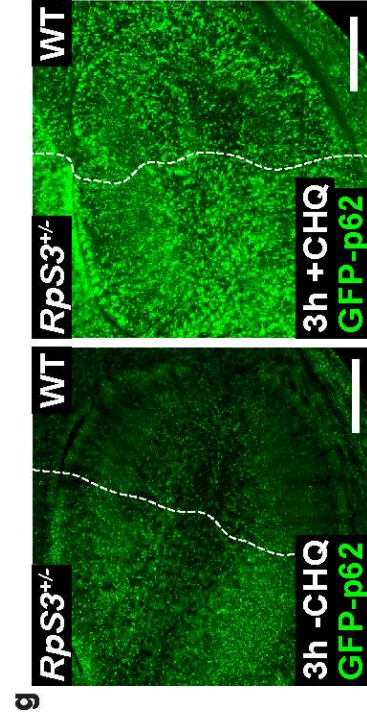
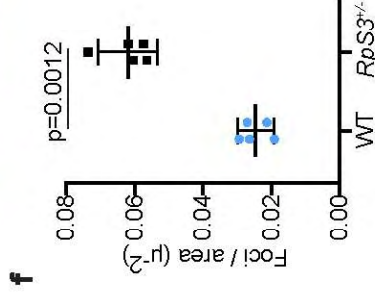
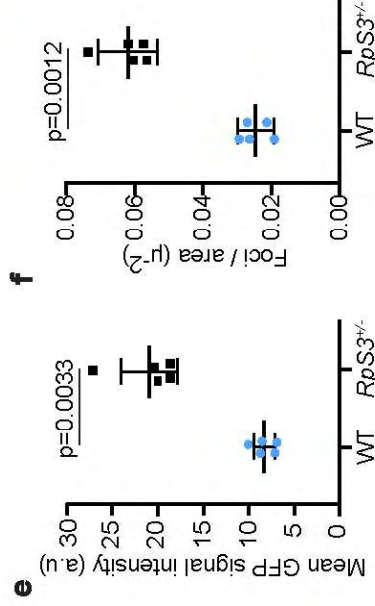
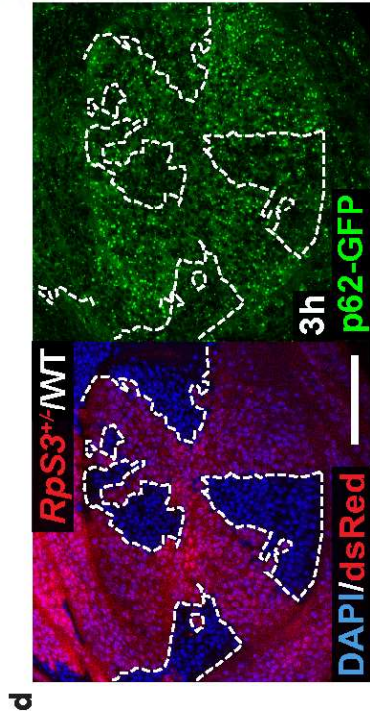
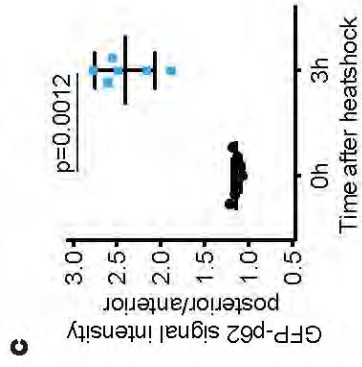
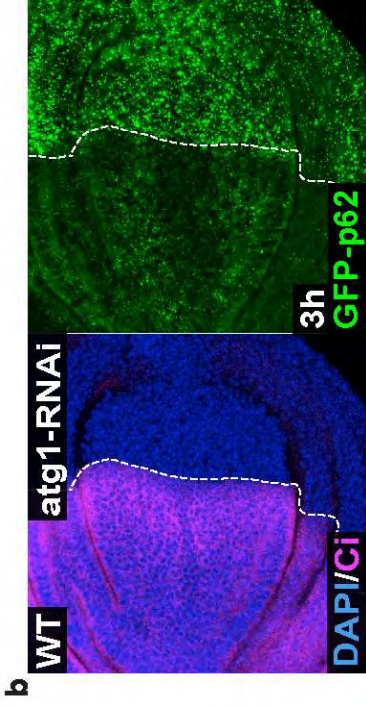
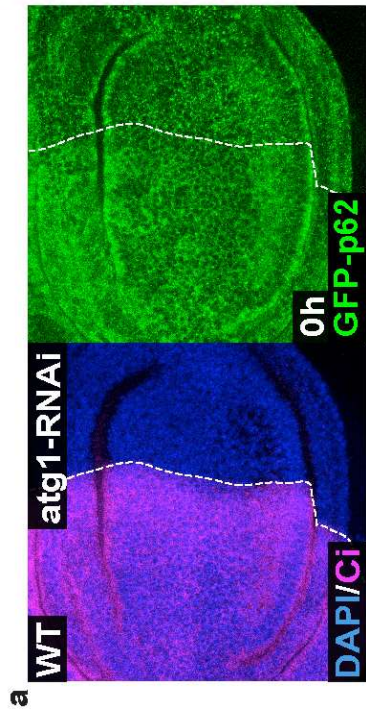




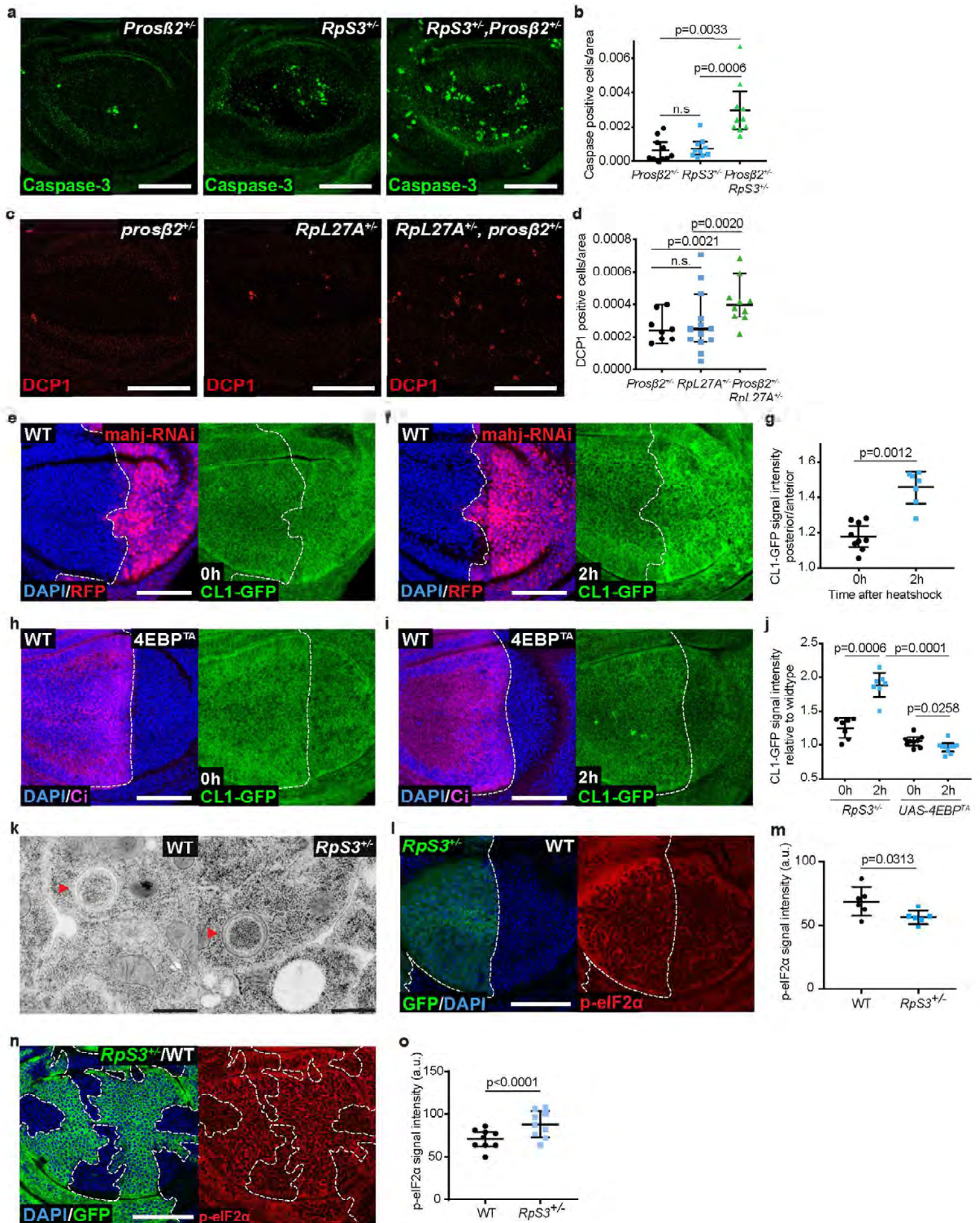




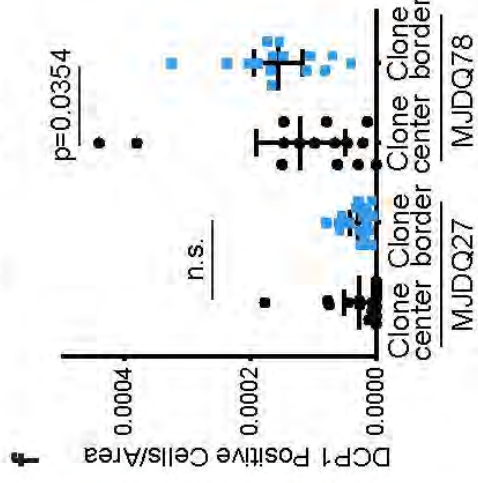
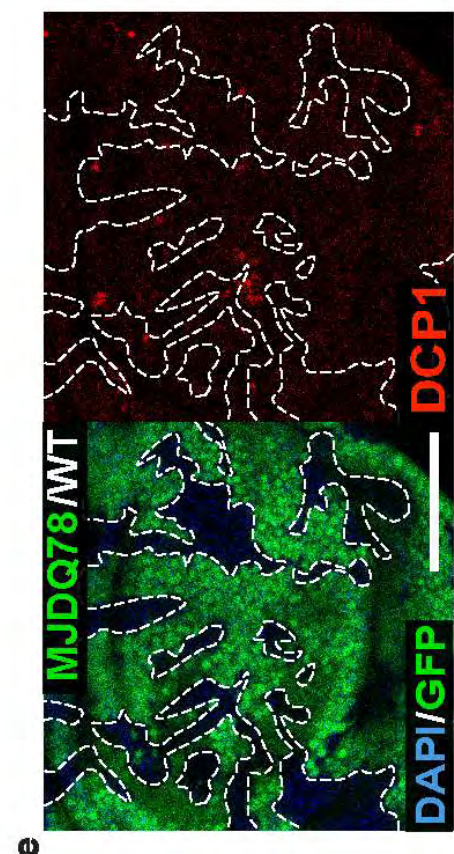
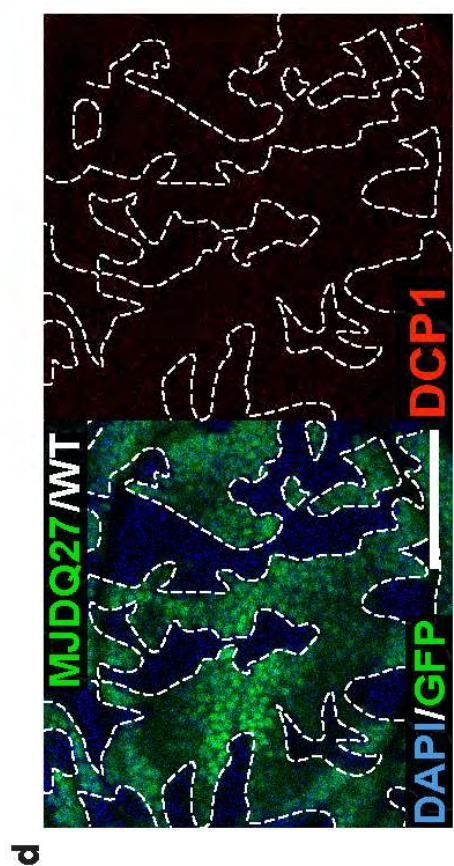
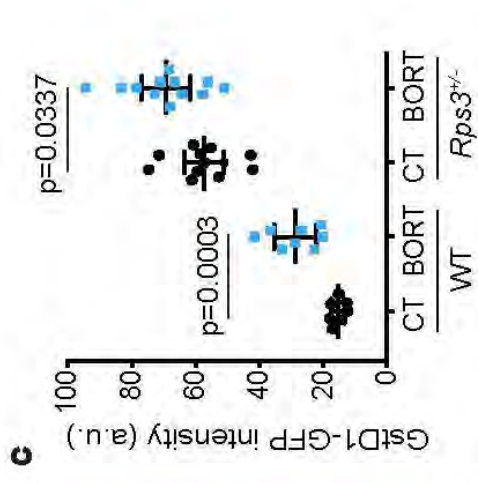
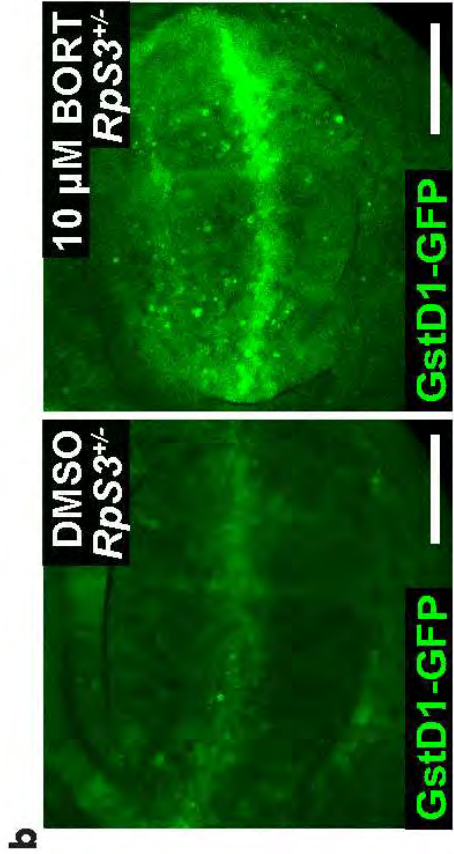
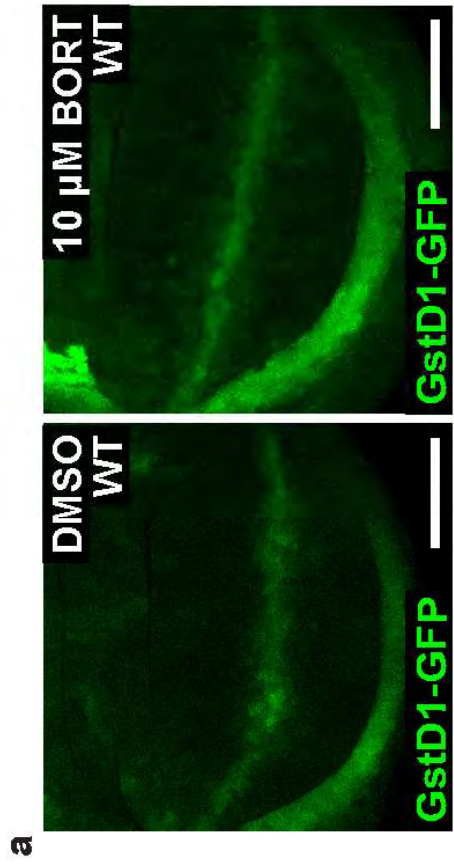












**Supplementary Table 1: Genes Differentially Expressed in JNK-inhibited vs JNK-Competent *R* and/or Unfolded Protein Res**

Flybase ID	baseMean	baseMeanA	baseMeanB	foldChange
FBgn0037363	729.9686512	857.895553	644.68405	0.75147149
FBgn0035871	2911.093424	2586.75265	3127.32061	1.20897551
FBgn0266717	3341.157454	4734.04767	2412.56398	0.50961971
FBgn0261108	614.6677406	738.832145	531.891471	0.71990841
FBgn0041171	3087.252066	3669.84514	2698.85669	0.73541433
FBgn0001229	242.6957176	84.5314897	348.138536	4.1184479
FBgn0038651	1517.545637	1780.8894	1341.98313	0.75354658
FBgn0004177	12456.47849	13894.5896	11497.7378	0.82749747
FBgn0034691	502.8745858	580.559601	451.084576	0.77698237
FBgn0264357	1305.968171	1512.67977	1168.16044	0.77224569
FBgn0000546	1934.569955	2271.77143	1709.76897	0.75261487
FBgn0260936	2755.394797	3109.12439	2519.57507	0.81038092
FBgn0022027	700.6554139	581.62374	780.009864	1.34109014
FBgn0010638	5935.767143	4848.29158	6660.75085	1.37383463
FBgn0261014	12642.64026	14794.3629	11208.1585	0.75759657
FBgn0020618	40188.92389	32970.6391	45001.1138	1.36488449
FBgn0266411	2422.272403	3059.27533	1997.60379	0.65296633
FBgn0031049	3115.65665	2292.96574	3664.11726	1.59798168
FBgn0026317	1055.60221	1280.86342	905.428069	0.70688885
FBgn0029840	1143.327745	1440.76628	945.03539	0.65592553
FBgn0039969	1595.360121	1317.53832	1780.57466	1.35144051
FBgn0039966	362.7577252	286.643353	413.50064	1.44256142
FBgn0044452	872.3920328	1081.11765	733.241619	0.67822555
FBgn0039749	57.19633646	38.3390108	69.7678869	1.81976231
FBgn0034009	878.5676128	1033.3322	775.391222	0.75037943
FBgn0262656	2491.90582	3200.84293	2019.28108	0.63085916
FBgn0086357	11239.95786	9471.06641	12419.2188	1.31127988
FBgn0262516	282.1412346	330.820728	249.688239	0.75475392
FBgn0035542	304.7599756	464.949062	197.967252	0.42578267
FBgn0027492	4889.528189	5453.11827	4513.80147	0.82774685
FBgn0000257	443.8182671	557.015364	368.353536	0.6612987
FBgn0030812	1685.891616	2138.55849	1384.1137	0.64721807
FBgn0010303	1297.782669	1575.86644	1112.39349	0.70589325
FBgn0003079	1107.539098	1340.8124	952.02356	0.71003487
FBgn0043884	6175.468358	8001.56571	4958.07013	0.61963749
FBgn0003392	2227.686666	2546.97911	2014.82504	0.79106461
FBgn0023143	13899.65	16296.4639	12301.7741	0.75487383
FBgn0038816	481.1665917	655.647881	364.845732	0.55646597
FBgn0005198	1208.354591	1454.30437	1044.38808	0.71813583
FBgn0040491	11.4673959	21.1199382	5.03236767	0.23827568
FBgn0021796	1955.828633	2334.81583	1703.17051	0.72946675
FBgn0052350	1014.219166	1174.01528	907.688424	0.77314873
FBgn0260439	9409.874135	10769.1083	8503.718	0.78963994
FBgn0265988	564.5226888	710.922878	466.922563	0.65678371
FBgn0025802	635.2609425	767.870222	546.854756	0.71217081

FBgn0032200	2663.448018	2277.65183	2920.64548	1.2823055
FBgn0000346	267.6667287	339.258002	219.939213	0.64829484
FBgn0035871	2911.093424	2586.75265	3127.32061	1.20897551
FBgn0001230	1544.760194	327.799689	2356.0672	7.18752115
FBgn0032480	987.0020988	1187.17181	853.555626	0.71898239
FBgn0051414	33.97843758	50.1062788	23.2265434	0.46354557
FBgn0051354	2053.897594	386.437015	3165.53798	8.19160137
FBgn0030873	1372.52166	1164.31162	1511.32836	1.29804455
FBgn0023511	966.9396468	1154.78757	841.707698	0.72888531
FBgn0013279	2000.731479	374.043904	3085.18986	8.24820248
FBgn0013278	2349.220237	394.518599	3652.35466	9.25775026
FBgn0013277	1804.670991	429.024649	2721.76855	6.34408434
FBgn0013276	3593.796257	921.628993	5375.2411	5.83232639
FBgn0013275	3460.852546	899.12626	5168.67007	5.74854756
FBgn0261984	932.6959586	1105.67106	817.379225	0.73926076
FBgn0047135	4792.886195	4050.44202	5287.84898	1.30549924
FBgn0028692	6176.020089	6941.31724	5665.82199	0.81624594
FBgn0028694	4538.980647	3996.40724	4900.69625	1.22627549
FBgn0032884	2741.779234	2124.16791	3153.52012	1.48459079
FBgn0250843	5528.735543	4849.85045	5981.3256	1.23330104
FBgn0036136	1271.155611	1449.28439	1152.40309	0.79515318
FBgn0086134	5568.679942	4780.63934	6094.04034	1.27473334
FBgn0033698	1598.10726	2005.84529	1326.28191	0.66120848
FBgn0023174	4969.922245	4291.74185	5422.04251	1.26336641
FBgn0028688	3401.475306	2980.25384	3682.28962	1.23556241
FBgn0028687	4008.243903	3308.35749	4474.83485	1.35258504
FBgn0016756	2814.273551	3911.47479	2082.80606	0.53248613
FBgn0031652	172.9232895	138.684144	195.749387	1.41147633
FBgn0261456	1813.781009	2090.78597	1629.11103	0.77918594
FBgn0031528	16.33450531	3.4431678	24.9287303	7.24005677
FBgn0259685	4027.850445	4748.12283	3547.66886	0.74717293
FBgn0030674	4286.686499	5970.40066	3164.21039	0.52998292
FBgn0036913	637.0777616	776.216957	544.318298	0.70124505
FBgn0266717	3341.157454	4734.04767	2412.56398	0.50961971
FBgn0028692	6176.020089	6941.31724	5665.82199	0.81624594
FBgn0028694	4538.980647	3996.40724	4900.69625	1.22627549
FBgn0028500	1082.883681	1232.45536	983.169229	0.79773212
FBgn0041171	3087.252066	3669.84514	2698.85669	0.73541433
FBgn0028467	505.7955589	602.373286	441.410408	0.7327855
FBgn0038660	1160.591245	1347.06643	1036.27446	0.76928237
FBgn0032884	2741.779234	2124.16791	3153.52012	1.48459079
FBgn0250848	6974.25661	5917.34448	7678.8647	1.29768762
FBgn0029996	1730.019475	2093.94929	1487.3996	0.7103322
FBgn0039214	2289.76443	2965.70159	1839.13966	0.62013645
FBgn0032480	987.0020988	1187.17181	853.555626	0.71898239
FBgn0032467	2075.514867	2361.39727	1884.9266	0.79822511
FBgn0250843	5528.735543	4849.85045	5981.3256	1.23330104
FBgn0017418	1028.689886	1252.30568	879.612692	0.70239456
FBgn0052850	822.0384789	620.988087	956.072074	1.53959809
FBgn0260962	4139.169281	4761.34196	3724.3875	0.78221382
FBgn0260940	531.5854584	452.795234	584.112275	1.29001419
FBgn0260936	2755.394797	3109.12439	2519.57507	0.81038092

FBgn0037842	575.5070859	483.78051	636.658136	1.31600617
FBgn0022027	700.6554139	581.62374	780.009864	1.34109014
FBgn0026597	2358.912377	2641.94034	2170.22707	0.82145196
FBgn0261014	12642.64026	14794.3629	11208.1585	0.75759657
FBgn0031107	1205.842386	1652.37955	908.150941	0.5496019
FBgn0000273	1822.114502	2057.40227	1665.25599	0.80939737
FBgn0031057	4034.45473	4711.82626	3582.87371	0.76040022
FBgn0024222	515.1267583	600.296744	458.346768	0.76353366
FBgn0029763	1621.906113	1884.32848	1446.95787	0.76789046
FBgn0029856	297.8690754	460.516126	189.437708	0.41135955
FBgn0086558	9639.740828	7078.04656	11347.537	1.6032018
FBgn0030320	1842.066755	2105.27179	1666.59673	0.7916302
FBgn0004391	1379.723421	1553.76644	1263.69474	0.81331062
FBgn0036136	1271.155611	1449.28439	1152.40309	0.79515318
FBgn0039749	57.19633646	38.3390108	69.7678869	1.81976231
FBgn0034071	1426.761309	1715.40778	1234.33033	0.71955505
FBgn0259174	1717.01028	2114.58566	1451.96003	0.68664044
FBgn0259152	1297.471767	1684.62622	1039.3688	0.61697295
FBgn0262517	1730.374145	1982.83312	1562.06816	0.78779608
FBgn0086134	5568.679942	4780.63934	6094.04034	1.27473334
FBgn0029093	4705.185504	3961.70571	5200.8387	1.31277765
FBgn0032208	4105.170465	4693.98134	3712.62988	0.79093409
FBgn0028476	1105.880312	1312.68972	968.007372	0.73742283
FBgn0030057	963.6034972	665.298037	1162.4738	1.74729781
FBgn0040291	148.3632378	106.160863	176.498155	1.66255389
FBgn0015024	6003.6949	7186.871	5214.91083	0.72561631
FBgn0050421	605.1824832	705.074813	538.587597	0.76387298
FBgn0003557	1152.955202	1307.08594	1050.20138	0.80346773
FBgn0260794	4560.851195	6389.26865	3341.90623	0.52304988
FBgn0037659	2480.722788	2938.46196	2175.56334	0.74037485
FBgn0030873	1372.52166	1164.31162	1511.32836	1.29804455
FBgn0030809	2826.576425	3478.47814	2391.97528	0.68764994
FBgn0005632	3734.308077	4956.79414	2919.31737	0.58895272
FBgn0261786	782.6120388	909.633609	697.930992	0.76726606
FBgn0033916	550.2156991	652.976065	481.708789	0.73771278
FBgn0023511	966.9396468	1154.78757	841.707698	0.72888531
FBgn0033738	890.031137	1016.77777	805.533381	0.79224134
FBgn0023174	4969.922245	4291.74185	5422.04251	1.26336641
FBgn0011706	274.6842702	368.283145	212.28502	0.57641796
FBgn0028688	3401.475306	2980.25384	3682.28962	1.23556241
FBgn0028687	4008.243903	3308.35749	4474.83485	1.35258504
FBgn0261931	684.5089227	884.467295	551.203341	0.62320376
FBgn0033260	2069.158216	2388.32647	1856.37938	0.77727204
FBgn0025720	1532.715771	1283.41383	1698.91707	1.32374845
FBgn0035959	611.2413624	742.891455	523.474634	0.70464485
FBgn0030366	3276.640922	4031.90482	2773.13165	0.6877969
FBgn0011230	5903.143503	6897.08343	5240.51689	0.75981637
FBgn0003942	35392.17608	29701.3805	39186.0398	1.31933396
FBgn0003941	33670.76822	28941.8432	36823.3849	1.27232342
FBgn0021796	1955.828633	2334.81583	1703.17051	0.72946675
FBgn0027053	2092.358829	1817.66131	2275.49051	1.25187817
FBgn0032640	3282.86616	2896.57778	3540.39175	1.22226711



FBgn0020257	4191.510026	4822.1305	3771.09638	0.78203947
FBgn0015589	985.108809	1254.94839	805.215754	0.64163257
FBgn0027512	1127.371706	1284.17078	1022.83899	0.79649764
FBgn0027508	1229.600297	1471.18068	1068.54671	0.72631915

---

**pS3<sup>+/-</sup> Cells With Associated With Protein Catabolism, Proteasome, Autophagy, ponce GO Terms**

log2FoldChange	pval	padj	symbol	GO
-0.412209721	0.003964	0.027398915	Atg17	GOBP:autophagy
0.273785023	0.00838	0.048419233	Bl-1	GOBP:autophagy
-0.972507034	1.93E-14	3.25E-12	Bruce	GOBP:autophagy
-0.474114733	0.000147	0.002057175	Atg13	GOBP:autophagy
-0.443370815	0.008303	0.048057042	ago	GOBP:autophagy
2.042100739	1.18E-28	6.21E-26	Hsp67Bc	GOBP:autophagy
-0.408231396	0.00016	0.002208433	CG14299	GOBP:autophagy
-0.273173192	0.00459	0.030501137	mts	GOBP:autophagy
-0.364046226	0.00547	0.034787939	Synj	GOBP:autophagy
-0.372868182	0.002554	0.019662639	SNF4Agam1	GOBP:autophagy
-0.410016292	0.000883	0.008676736	EcR	GOBP:autophagy
-0.303327892	0.00305	0.022496927	scny	GOBP:autophagy
0.423406212	0.000717	0.007394443	Vps25	GOBP:autophagy
0.458208351	5.06E-06	0.000125619	Sec61beta	GOBP:autophagy
-0.400498301	3.15E-05	0.000589822	TER94	GOBP:autophagy
0.448778858	3.82E-05	0.000682303	Rack1	GOBP:autophagy
-0.614919488	0.000188	0.002513911	sima	GOBP:autophagy
0.676250872	8.68E-06	0.000200474	Sec61gamn	GOBP:autophagy
-0.500444712	1.01E-05	0.000227807	Tsc1	GOBP:autophagy
-0.608396057	5.23E-08	2.60E-06	raptor	GOBP:autophagy
0.434498005	7.94E-05	0.001245118	Fis1	GOBP:autophagy
0.528632741	0.000329	0.004012845	Rab21	GOBP:autophagy
-0.560162952	1.62E-06	4.82E-05	Atg2	GOBP:autophagy
0.863750027	0.004731	0.031262995	CG11498	GOBP:autophagy
-0.414307824	0.000391	0.004577633	CG8155	GOBP:autophagy
-0.664610139	9.83E-05	0.001483762	dm	GOBP:autophagy
0.390975647	0.002947	0.021935815	Sec61alpha	GOBP:autophagy
-0.40592176	0.008509	0.048982772	Trpml	GOBP:autophagy
-1.231810872	5.09E-13	7.10E-11	DOR	GOBP:autophagy
-0.272738479	0.005937	0.0370168	wdb	GOBP:autophagy
-0.59662603	9.52E-06	0.000215946	car	GOBP:autophagy
-0.627676211	9.92E-08	4.51E-06	CG8949	GOBP:autophagy
-0.502478068	5.01E-06	0.000124903	hep	GOBP:autophagy
-0.494038218	1.12E-05	0.000249157	phl	GOBP:autophagy
-0.690503651	6.35E-08	3.11E-06	mask	GOBP:autophagy
-0.338132559	0.00117	0.010802171	shi	GOBP:autophagy
-0.405692562	2.39E-05	0.000468987	Uba1	GOBP:autophagy
-0.845634638	9.39E-06	0.000214176	Lrrk	GOBP:autophagy
-0.477671347	1.75E-05	0.000360907	gig	GOBP:autophagy
-2.069296379	0.001318	0.011812175	Buffy	GOBP:autophagy
-0.45508588	1.50E-05	0.000318585	Tor	GOBP:autophagy
-0.371182122	0.001147	0.010677893	CG32350	GOBP:autophagy
-0.340733141	0.000436	0.004960801	Pp2A-29B	GOBP:autophagy
-0.606509757	2.18E-05	0.000434278	mv	GOBP:autophagy
-0.489704796	8.20E-05	0.0012798	Sbf	GOBP:autophagy

0.358740016	0.001689	0.014278517	CG5676	GOBP:autophagy
-0.625277998	6.10E-05	0.001003835	comt	GOBP:autophagy
0.273785023	0.00838	0.048419233	Bl-1	GOBP:response_to_unfolded_protein
2.845494297	2.75E-112	3.33E-108	Hsp68	GOBP:response_to_unfolded_protein
-0.475971657	0.000108	0.001593513	Edem2	GOBP:response_to_unfolded_protein
-1.10921693	0.007779	0.04577929	CG31414	GOBP:response_to_unfolded_protein
3.034145511	2.47E-52	2.73E-49	Hsp70Bbb	GOBP:response_to_unfolded_protein
0.376339903	0.000735	0.007509983	CG15814	GOBP:response_to_unfolded_protein
-0.456236267	7.13E-05	0.001140905	Edem1	GOBP:response_to_unfolded_protein
3.04407975	2.16E-39	1.54E-36	Hsp70Bc	GOBP:response_to_unfolded_protein
3.210661644	1.26E-40	1.02E-37	Hsp70Bb	GOBP:response_to_unfolded_protein
2.66541195	3.99E-50	3.73E-47	Hsp70Ba	GOBP:response_to_unfolded_protein
2.544071459	3.91E-10	3.32E-08	Hsp70Ab	GOBP:response_to_unfolded_protein
2.523197488	1.03E-10	9.80E-09	Hsp70Aa	GOBP:response_to_unfolded_protein
-0.435844761	0.002396	0.018735455	Ire1	GOBP:response_to_unfolded_protein
0.384601618	0.00332	0.024004011	CG32276	GOBP:response_to_unfolded_protein
-0.292924192	0.002865	0.021522664	Rpn2	GOCC:proteasome_complex
0.294283128	0.003656	0.025819057	Rpn11	GOCC:proteasome_complex
0.570065321	0.000333	0.004052621	Pomp	GOCC:proteasome_complex
0.302524993	0.003708	0.026048442	Prosalph6	GOCC:proteasome_complex
-0.330695285	0.002715	0.020584763	Ufd1-like	GOCC:proteasome_complex
0.35019548	0.001575	0.013490523	Prosalph2	GOCC:proteasome_complex
-0.596822876	2.48E-08	1.35E-06	CG8858	GOCC:proteasome_complex
0.337273124	0.001058	0.010020919	Prosbeta2	GOCC:proteasome_complex
0.305167883	0.002966	0.0220384	Rpn7	GOCC:proteasome_complex
0.435719304	1.99E-05	0.000402553	Rpt1	GOCC:proteasome_complex
-0.909184157	3.54E-19	1.13E-16	Ubp64E	GOBP:protein_catabolic_process
0.497204939	0.008086	0.047172659	jet	GOBP:protein_catabolic_process
-0.359960453	0.000671	0.007003891	hpo	GOBP:protein_catabolic_process
2.85600101	1.93E-05	0.000392329	CG15412	GOBP:protein_catabolic_process
-0.420485904	0.00567	0.035726545	crb	GOBP:protein_catabolic_process
-0.915982222	8.92E-17	1.90E-14	CG8184	GOBP:protein_catabolic_process
-0.512009417	0.00011	0.001625111	CG8334	GOBP:protein_catabolic_process
-0.972507034	1.93E-14	3.25E-12	Bruce	GOBP:protein_catabolic_process
-0.292924192	0.002865	0.021522664	Rpn2	GOBP:protein_catabolic_process
0.294283128	0.003656	0.025819057	Rpn11	GOBP:protein_catabolic_process
-0.326023723	0.003913	0.027124108	Rich	GOBP:protein_catabolic_process
-0.443370815	0.008303	0.048057042	ago	GOBP:protein_catabolic_process
-0.448537143	0.00062	0.006616451	CG11070	GOBP:protein_catabolic_process
-0.37841485	0.000723	0.007426578	CG14291	GOBP:protein_catabolic_process
0.570065321	0.000333	0.004052621	Pomp	GOBP:protein_catabolic_process
0.375943142	0.000159	0.002192274	26-29-p	GOBP:protein_catabolic_process
-0.493434215	3.44E-06	9.07E-05	UbcE2H	GOBP:protein_catabolic_process
-0.6893424	2.61E-11	2.73E-09	puf	GOBP:protein_catabolic_process
-0.475971657	0.000108	0.001593513	Edem2	GOBP:protein_catabolic_process
-0.325132428	0.00383	0.026753656	CG9934	GOBP:protein_catabolic_process
0.302524993	0.003708	0.026048442	Prosalph6	GOBP:protein_catabolic_process
-0.509646429	7.60E-06	0.000178	ari-1	GOBP:protein_catabolic_process
0.622553789	3.33E-07	1.28E-05	CG32850	GOBP:protein_catabolic_process
-0.354365064	0.000387	0.004540581	pic	GOBP:protein_catabolic_process
0.367386932	0.005592	0.035393781	lsn	GOBP:protein_catabolic_process
-0.303327892	0.00305	0.022496927	scny	GOBP:protein_catabolic_process

0.396166253	0.002407	0.018778946	CG6567	GOBP:protein_catabolic_process
0.423406212	0.000717	0.007394443	Vps25	GOBP:protein_catabolic_process
-0.28375189	0.006264	0.03866191	Axn	GOBP:protein_catabolic_process
-0.400498301	3.15E-05	0.000589822	TER94	GOBP:protein_catabolic_process
-0.863541106	6.49E-15	1.21E-12	HERC2	GOBP:protein_catabolic_process
-0.305079928	0.004051	0.027851465	Pka-C1	GOBP:protein_catabolic_process
-0.395169149	7.50E-05	0.001190318	Ubqn	GOBP:protein_catabolic_process
-0.389236345	0.002845	0.021419809	ird5	GOBP:protein_catabolic_process
-0.381027569	0.000384	0.004521274	CG4165	GOBP:protein_catabolic_process
-1.281528146	2.03E-11	2.20E-09	CG11700	GOBP:protein_catabolic_process
0.680956037	1.29E-08	7.61E-07	Ubi-p5E	GOBP:protein_catabolic_process
-0.337101445	0.00147	0.012823147	CG2247	GOBP:protein_catabolic_process
-0.298121644	0.006585	0.040051633	shtd	GOBP:protein_catabolic_process
-0.330695285	0.002715	0.020584763	Ufd1-like	GOBP:protein_catabolic_process
0.863750027	0.004731	0.031262995	CG11498	GOBP:protein_catabolic_process
-0.47482303	2.72E-05	0.00052288	CG8405	GOBP:protein_catabolic_process
-0.542373269	3.49E-07	1.33E-05	Nedd4	GOBP:protein_catabolic_process
-0.696720862	2.25E-10	2.04E-08	Clbn	GOBP:protein_catabolic_process
-0.344105857	0.001266	0.011488039	l(3)76BDr	GOBP:protein_catabolic_process
0.35019548	0.001575	0.013490523	Prosalph2	GOBP:protein_catabolic_process
0.392622579	0.000105	0.001565251	cathD	GOBP:protein_catabolic_process
-0.33837061	0.001889	0.015603996	CG5604	GOBP:protein_catabolic_process
-0.43943601	0.000936	0.009080583	CG15817	GOBP:protein_catabolic_process
0.805125523	1.59E-11	1.77E-09	Ppt1	GOBP:protein_catabolic_process
0.733401102	0.003533	0.025186264	Roc1b	GOBP:protein_catabolic_process
-0.462721205	2.32E-05	0.00045621	Cklalpha	GOBP:protein_catabolic_process
-0.388595337	0.004186	0.028370974	CG30421	GOBP:protein_catabolic_process
-0.315688011	0.004911	0.032051704	Su(dx)	GOBP:protein_catabolic_process
-0.934979551	3.44E-08	1.79E-06	ctrip	GOBP:protein_catabolic_process
-0.433672206	2.57E-05	0.000500275	Kdm2	GOBP:protein_catabolic_process
0.376339903	0.000735	0.007509983	CG15814	GOBP:protein_catabolic_process
-0.540253771	0.000656	0.006883543	CG9086	GOBP:protein_catabolic_process
-0.763776283	7.21E-14	1.14E-11	faf	GOBP:protein_catabolic_process
-0.382201162	0.001387	0.012266678	mi	GOBP:protein_catabolic_process
-0.438868864	0.000638	0.00677159	CG8494	GOBP:protein_catabolic_process
-0.456236267	7.13E-05	0.001140905	Edem1	GOBP:protein_catabolic_process
-0.335988117	0.004056	0.027851465	DUBAI	GOBP:protein_catabolic_process
0.337273124	0.001058	0.010020919	Prosbeta2	GOBP:protein_catabolic_process
-0.7948128	2.63E-07	1.06E-05	rpr	GOBP:protein_catabolic_process
0.305167883	0.002966	0.0220384	Rpn7	GOBP:protein_catabolic_process
0.435719304	1.99E-05	0.000402553	Rpt1	GOBP:protein_catabolic_process
-0.682224165	2.33E-08	1.27E-06	CG42797	GOBP:protein_catabolic_process
-0.363508479	0.000511	0.005640119	Cul4	GOBP:protein_catabolic_process
0.404628996	0.00024	0.003077717	Ate1	GOBP:protein_catabolic_process
-0.5050318	5.55E-05	0.000925226	CG4911	GOBP:protein_catabolic_process
-0.539945473	8.63E-08	4.03E-06	Usp7	GOBP:protein_catabolic_process
-0.396277303	5.42E-05	0.000911322	poe	GOBP:protein_catabolic_process
0.399809793	0.001669	0.014145039	RpS27A	GOBP:protein_catabolic_process
0.347465445	0.004075	0.027872041	RpL40	GOBP:protein_catabolic_process
-0.45508588	1.50E-05	0.000318585	Tor	GOBP:protein_catabolic_process
0.324094167	0.002378	0.018624095	CSN5	GOBP:protein_catabolic_process
0.2895596	0.004894	0.032027097	Sgt	GOBP:protein_catabolic_process

-0.354686674	0.000382	0.004503224	ppa	GOBP:protein_catabolic_process
-0.64018073	1.46E-07	6.28E-06	Apc	GOBP:protein_catabolic_process
-0.328258016	0.003584	0.025441752	CG10254	GOBP:protein_catabolic_process
-0.461324471	0.00022	0.002883496	Tnks	GOBP:protein_catabolic_process

---

**Supplementary Table 2: Key Experimental Resources**

Antibodies		
Rabbit anti-pJNK pTPpY (used 1:500)	Promega	Cat#V793B
Rat anti-Ci (used 1:1000)	DSHB	Cat#2A1
Rabbit anti-Ref(2)P (used 1:2000)	Tor Erik Rusten <sup>63</sup>	N/A
Rabbit anti-cleaved Caspase-3 (used 1:25000)	Abcam	Cat#13847
Rabbit anti-Dcp1 (used 1:2500)	Cell signalling	Cat#9578S
Rabbit anti-p-eif2 $\alpha$ (used 1:500)	Cell signaling	Cat#3398T
Mouse anti-FK2 (used 1:5000)	Merck	Cat#04-263
Drosophila Strains		
<i>Drosophila RpS3[Plac92]</i>	Bloomington	Cat#BL5627
<i>Drosophila RpS3*</i>	Bloomington	Cat#BL5699
<i>Drosophila RpL27A[1]</i>	Bloomington	Cat#BL5697
<i>Drosophila hs-FLP;; FRT82B</i>	Daniel St. Johnston	N/A
<i>y [1],w[1118]</i>	Daniel St. Johnston	N/A
<i>en-Gal4, UAS-FLP; FRT82B</i>	24	N/A
<i>hh-Gal4/TM6b</i>	Jean-Paul Vincent	N/A
<i>Drosophila FRT42D, ubi-GFP/Cyo</i>	Bloomington	Cat#BL5697
<i>FRT82B, RpS3[Plac92], hh-Gal4</i>	24	N/A
<i>Drosophila hs-FLP, UAS-CD8-GFP;; FRT82B, RpS3[Plac92], act&gt;RpS3&gt;Gal4/TM6b</i>	This paper	N/A
<i>Drosophila tub-Gal80<sup>TS</sup></i>	Bloomington	Cat#BL7016
<i>Drosophila UAS-GFP-atg8-mCherry</i>	Bloomington	Cat#BL37749
<i>Drosophila FRT42D mahj</i>	31	N/A
<i>Drosophila UAS-puc</i>	E. Martinez Blanco	N/A
<i>Drosophila UAS-4E-BP<sup>TA</sup></i>	29	N/A
<i>Drosophila w+/w-; tub&gt;CD2&gt;Gal4, UAS-GFP; tub-Gal80<sup>TS</sup></i>	Bruce Edgar	N/A
<i>Drosophila hs-FLP<sup>122</sup>;; act&gt;CD2&gt;Gal4, UAS-GFP/TM6b</i>	Bruce Edgar	N/A
<i>Drosophila UAS-GADD34</i>	FlyORF	Cat#F003018
<i>Drosophila UAS-dFOXO</i>	Bloomington	Cat#BL9575

<i>Drosophila</i> <i>Pros β2<sup>EP3067</sup>/TM6b</i>	Bloomington	Cat#BL6787
<i>Drosophila UASp-GFP- mCherry-Atg8a</i>	Bloomington	Cat#BL37749
<i>Drosophila hslp;; FRT82B atg13/TM6b</i>	Tor Erik Rusten	N/A
<i>Drosophila UAS-Atg1 RNAi</i>	Harvard TRiP	HMS02750
<i>Drosophila UAS-Atg9-RNAi</i>	Bloomington	Cat#BL28055
<i>Drosophila UAS-p62-RNAi</i>	Bloomington	Cat#BL33978
<i>Drosophila UAS-Rpt6 RNAi</i>	VDRC	Cat#49244/GD
<i>Drosophila</i> <i>Atg8a<sup>KG07569</sup>/FM7c</i>	Bloomington	Cat#BL14639
<i>Drosophila Ref(2)P<sup>od2</sup>/CyO</i>	64	N/A
<i>Drosophila UAS-mahj RNAi</i>	Bloomington	Cat#BL34912
<i>Drosophila GstD1-GFP</i>	33	N/A
<i>Drosophila hs-CL1-GFP (ProteoFLUX)</i>	This paper	N/A
<i>Drosophila hs-p62- GFP(ReFLUX)</i>	This paper	N/A
<i>Drosophila UAS-Hsap/MJD- Q27</i>	Bloomington	Cat#BL8149
<i>Drosophila UAS-Hsap/MJD- Q78</i>	Bloomington	Cat#BL8150
Oligonucleotides		
Primer: CAAGAAGAGAACTCTGAATA GGG	This paper	pUAST_p62_F1
Primer: CAAGTAAATCAACTGCAACTA CT	This paper	pUAST_p62_F2
Primer: GAGTATAAATAGAGCGTTC G	This paper	pUAST_p62_F3
Primer: CCATTCATCAGTCCATAGG TG	This paper	pUAST_p62_R1
Primer: GTCACACCACAGAAGTAAGG TTC	This paper	pUAST_p62_R2
Primer: CAGAGAAGGAGGCAAACAG	This paper	pUAST_p62_R3
Primer: TGAATAGGGAATTGGGAATT CAATAGGGAATTGGGAATTC AGCGC	This paper	CL1-GFP_InfusF
Primer: GCTGGAATTAGGCCTTCTAG CGGCGGCAGATCCTCAC	This paper	CL1-GFP_InfusR

Primer: TCGATCCCCGGGTACCCGGC GATCTTGAAGTTCCTATTCC AAGTTCCTATTCCGAAGTTC TATTCTCTAGAAAGTATAGGA ACTTCAGAGCGCTTCAAATG AATGCCAACCTTCCGATTC	This paper	RpS3_FusL
CTGCCTTTTTACAAAACCTTC CCTCGGACAGA	This paper	RpS3_FusR
TTTGTA AAAAGGCAGATCGAA TTCGAGCT	This paper	$\alpha$ T_H70_FusL
TCCCGGATCTGGTACCAGCT CAAAGCGCTCTGAAGT	This paper	$\alpha$ T_H70_FusR



**Supplementary Table 3: Experimental Genotypes and Conditions**

Figure/Panel	Genotype	Heat shock duration, time between heat shock and dissection (water bath temperature)
<b>Main figures</b>		
1a (left)	<i>yw</i>	N/A
1a (right)	<i>FRT82B, RpS3[Plac92], ubi-GFP/+</i>	N/A
1c	<i>hs-FLP;; FRT82B, RpS3[Plac92], ubi-GFP/FRT82B</i>	10 min, 72 hours
1e	<i>hs-FLP;; FRT82B, RpS3[Plac92], ubi-GFP/FRT82B</i>	10 min, 72 hours
1f	<i>hs-FLP; tub&gt;CD2&gt;Gal4, UAS-CD8-GFP/+; tub-Gal80<sup>TS</sup>/UAS-4E-BP<sup>TA</sup></i>	40 min, 72 hours (29 °C)
1h	<i>hs-FLP; tub&gt;CD2&gt;Gal4, UAS-CD8-GFP/+; tub-Gal80<sup>TS</sup>/UAS-4E-BP<sup>TA</sup></i>	40 min, 72 hours (29 °C)
1j	<i>en-Gal4, UAS-FLP/+; FRT82B, RpS3[Plac92], ubi-GFP/FRT82B</i>	N/A
1k	<i>hh-Gal4/UAS-4E-BP<sup>TA</sup></i>	N/A
1l	<i>en-Gal4, UAS-FLP/GstD1-GFP; FRT82B, RpS3[Plac92], tub-dsRed/FRT82B</i>	N/A
1m	<i>GstD1-GFP/+; hh-Gal4/UAS-4E-BP<sup>TA</sup></i>	N/A
1o	<i>GstD1-GFP/+; FRT82B, RpS3[Plac92], hh-Gal4/UAS-GADD34</i>	N/A
1q	<i>hs-FLP, UAS-CD8-GFP/+;; FRT82B, RpS3[Plac92], act&gt;RpS3&gt;Gal4/+</i>	25 min, 72 hours
1r	<i>hs-FLP, UAS-CD8-GFP/+;; FRT82B, RpS3[Plac92], act&gt;RpS3&gt;Gal4/UAS-GADD34</i>	25 min, 72 hours
2a (left)	<i>p62<sup>pd2</sup> /+</i>	N/A
2a (middle)	<i>FRT82B, RpS3[Plac92], tub-dsRed/+</i>	N/A
2a (right)	<i>p62<sup>pd2</sup> /+; FRT82B, RpS3[Plac92], tub-dsRed/+</i>	N/A
2c (left)	<i>UAS-GFP-mCherry-atg8a/GstD1-GFP; hh-Gal4/+</i>	N/A
2c (right)	<i>UAS-GFP-mCherry-atg8a/+; hh-Gal4/FRT82B, RpS3[Plac92], ubi-GFP</i>	N/A
2d	<i>en-Gal4, UAS-FLP/+; FRT82B, RpS3[Plac92], tub-dsRed/FRT82B</i>	N/A
2f	<i>hs-FLP; FRT42D mahj/FRT42D, ubi-GFP</i>	1 hour, 72 hours
2g	<i>hh-Gal4/UAS-4E-BP<sup>TA</sup></i>	N/A
2i-j	<i>hs-GFP-p62/+; en-Gal4, UAS-FLP/+; FRT82B, RpS3[Plac92], tub-dsRed/FRT82B</i>	N/A
2l-m	<i>hs-GFP-p62/+; en-Gal4, UAS-RFP/+; tub-Gal80<sup>TS</sup>/UAS-mahj RNAi</i>	(27°C)
3a	<i>hs-FLP; UAS-atg1 RNAi/+; act&gt;CD2&gt;Gal4, UAS-GFP/+</i>	40 min, 72 hours
3c	<i>hs-FLP; UAS-atg1 RNAi/+; act&gt;CD2&gt;Gal4, UAS-GFP/+</i>	40 min, 72 hours
3d	<i>GstD1-GFP/UAS-atg1 RNAi; hh-Gal4/+</i>	N/A
3e-f	<i>hs-FLP;; FRT82B atg13/FRT82B ubi-GFP</i>	25 min, 72 hours
3j	<i>hs-FLP; tub&gt;CD2&gt;Gal4, UAS-CD8-GFP/+; UAS-Atg9-RNAi/+</i>	40 min, 72 hours
3k	<i>hs-FLP; tub&gt;CD2&gt;Gal4, UAS-CD8-GFP/+; UAS-Atg9-RNAi/UAS-4E-BP<sup>TA</sup></i>	40 min, 72 hours
4a	<i>yw</i>	N/A

4b	<i>FRT82B, RpS3[Plac92], ubi-GFP/+</i>	N/A
4e	<i>hs-CL1-GFP/+; en-Gal4, UAS-RFP/UAS-Rpt6 RNAi; Gal80<sup>TS</sup>/+</i>	(29°C)
4g-h	<i>hs-CL1-GFP/+; en-Gal4, UAS-FLP/+; FRT82B, RpS3[Plac92], tub-dsRed/FRT82B</i>	N/A
4k	<i>en-Gal4, UAS-FLP/+; FRT82B, RpS3<sup>γ</sup>/FRT82B</i>	N/A
4l	<i>en-Gal4, UAS-FLP/+; FRT82B, RpS3[Plac92], ubi-GFP/FRT82B</i>	N/A
5a-b	<i>hs-FLP/+;; FRT82B, RpS3[Plac92], ubi-GFP/FRT82B</i>	12 min, 54 hours
5d-e	<i>GstD1-GFP/+; FRT82B, RpS3[Plac92], tub-dsRed/+</i>	N/A
5f	<i>tub-Gal80<sup>TS</sup>/+; UAS-dFOXO/+; FRT82B, RpS3[Plac92], hh-Gal4/+</i>	(27.5C)
5g	<i>hs-FLP; tub&gt;CD2&gt;Gal4, UAS-CD8-GFP/UAS-dFOXO; FRT82, RpS3[Plac92], tub-dsRed/+</i>	N/A
5i	<i>UAS-dFOXO/+; FRT82B, RpS3[Plac92], tub-dsRed/hh-Gal4, tub-Gal80</i>	(26.5°C)
5k	<i>hs-FLP, UAS-CD8-GFP/+;; FRT82B, RpS3[Plac92], act&gt;RpS3&gt;Gal4/+</i>	40 min, 72 hours
5l	<i>hs-FLP, UAS-CD8-GFP/+; UAS-dFOXO/+; FRT82B, RpS3[Plac92], act&gt;RpS3&gt;Gal4/+</i>	40 min, 72 hours
6a	<i>GstD1-GFP/UAS-MJDQ78; hh-Gal4/+</i>	N/A
6c	<i>hs-p62-GFP; UAS-MJDQ78/+; hh-Gal4/+</i>	N/A
6d	<i>GstD1-GFP/UAS-MJDQ78; hh-Gal4/+</i>	N/A
6f	<i>hs-FLP; UAS-MJDQ78/+; act&gt;CD2&gt;Gal4, UAS-GFP/+</i>	30 min, 72 hours
6h	<i>hs-FLP/+; tub&gt;CD2&gt;Gal4, UAS-CD8-GFP/UAS-MJDQ78</i>	40 min, 72 hours
6k	<i>hs-FLP;; act&gt;CD2&gt;Gal4, UAS-GFP/+</i>	12 min, 96 hours
6l	<i>hs-FLP; UAS-MJDQ78/+; act&gt;CD2&gt;Gal4, UAS-GFP/+</i>	12 min, 96 hours
<b>Extended data figures</b>		
ED1a	<i>hs-FLP;; FRT82B, RpS3[Plac92], ubi-GFP/FRT82B</i>	12 min, 48 hours
ED1b	<i>hs-FLP; tub&gt;CD2&gt;Gal4, UAS-CD8-GFP/+; tub-Gal80<sup>TS</sup>/UAS-4E-BP<sup>TA</sup></i>	40 min, 72 hours (29 °C)
ED1d	<i>en-Gal4, UAS-RFP/+; tub-Gal80<sup>S</sup>/UAS-mahj RNAi</i>	(27°C)
ED1f	<i>GstD1-GFP/+; FRT82B, RpS3[Plac92], hh-Gal4/UAS-GADD34</i>	N/A
ED1h	<i>GstD1-GFP/+; FRT82B, RpS3[Plac92], hh-Gal4/UAS-GADD34</i>	N/A
ED2a	<i>GstD1-GFP/+; FRT82B, RpS3[Plac92], Hh-Gal4/UAS-puc</i>	N/A
ED2b (left)	<i>Atg8a<sup>KG07569</sup> /+</i>	N/A
ED2b (middle)	<i>FRT82B, RpS3[Plac92], ubi-GFP/+</i>	N/A
ED2b (right)	<i>Atg8a<sup>KG07569</sup> /+;; FRT82B, RpS3[Plac92], ubi-GFP/+</i>	N/A
ED2d (left)	<i>FRT82B, atg13/+</i>	N/A
ED2d (middle)	<i>FRT82B, RpS3[Plac92], ubi-GFP/+</i>	N/A
ED2d (right)	<i>FRT82B, RpS3[Plac92], ubi-GFP/FRT82B atg13</i>	N/A
ED2f (left)	<i>p62<sup>pd2</sup> /+</i>	N/A
ED2f (middle)	<i>GFP, RpL27A[1], FRT40A+</i>	N/A
ED2f (right)	<i>p62<sup>pd2</sup> / GFP, RpL27A[1], FRT40A</i>	N/A

ED2h (left)	<i>hs-FLP, UAS-CD8-GFP/+;; FRT82B, RpS3[Plac92], act&gt;RpS3&gt;Gal4/+</i>	25 min, 72 hours
ED2h (middle)	<i>hs-FLP, UAS-CD8-GFP/+; UAS-Atg1 RNAi/+; FRT82B, RpS3[Plac92], act&gt;RpS3&gt;Gal4/+</i>	25 min, 72 hours
ED2h (right)	<i>hs-FLP, UAS-CD8-GFP/+;; FRT82B, RpS3[Plac92], act&gt;RpS3&gt;Gal4/UAS-Atg9 RNAi</i>	25 min, 72 hours
ED3a-b	<i>hs-GFP-p62/+; UAS-atg1 RNAi/+; hh-Gal4/+</i>	N/A
ED3d	<i>hs-FLP/hs-GFP-p62;; FRT82B, RpS3[Plac92], tub-dsRed/FRT82B</i>	15 min, 72 hours
ED3g-h	<i>hs-GFP-p62/+; en-Gal4, UAS-FLP/+; FRT82B, RpS3[Plac92], tub-dsRed/FRT82B</i>	N/A
ED3i-j	<i>hs-GFP-p62/+;; hh-Gal4/UAS-4E-BP<sup>A</sup></i>	N/A
ED4a (left)	<i>Prosβ2<sup>EP3067</sup> /+</i>	N/A
ED4a (middle)	<i>FRT82B, RpS3[Plac92], tub&gt;dsRed/+</i>	N/A
ED4a (right)	<i>FRT82B, RpS3[Plac92], tub&gt;dsRed/ Prosβ2<sup>EP3067</sup></i>	N/A
ED4c (left)	<i>Prosβ2<sup>EP3067</sup> /+</i>	N/A
ED4c (middle)	<i>GFP, RpL27A[1], FRT40A /+</i>	N/A
ED4c (right)	<i>GFP, RpL27A[1], FRT40A /+; Prosβ2<sup>EP3067</sup> /+</i>	N/A
ED4e-f	<i>hs-CL1-GFP; enGal4, UAS-RFP/+; tub-Gal80<sup>TS</sup>/UAS-mahj RNAi</i>	(27°C)
ED4h-i	<i>hs-CL1-GFP;; hh-Gal4/UAS-4E-BP<sup>A</sup></i>	N/A
ED4k	<i>en-Gal4, UAS-FLP/+; FRT82B, RpS3[Plac92], ubi-GFP/FRT82B</i>	N/A
ED4l	<i>en-Gal4, UAS-FLP/+; FRT82B, RpS3[Plac92], ubi-GFP/FRT82B</i>	N/A
ED4n	<i>hs-FLP, UAS-CD8-GFP/+;; FRT82B, RpS3[Plac92], act&gt;RpS3&gt;Gal4/+</i>	25min, 72 hours
ED5a	<i>yw, GstD1-GFP /+</i>	N/A
ED5b	<i>GstD1-GFP/+; FRT82B, RpS3[Plac92], tub-dsRed/+</i>	N/A
ED5d	<i>hs-FLP; UAS-MJDQ27/+; act&gt;CD2&gt;Gal4, UAS-GFP/+</i>	30min, 72 hours
ED5e	<i>hs-FLP; UAS-MJDQ78/+; act&gt;CD2&gt;Gal4, UAS-GFP/+</i>	30min, 72 hours